


# Intrinsic Mixed-State Topological Order

Zijian Wang<sup>1,†</sup>, Zhengzhi Wu,<sup>1,2,†</sup> and Zhong Wang<sup>1,\*</sup>

<sup>1</sup>*Institute for Advanced Study, Tsinghua University, Beijing 100084, People's Republic of China*

<sup>2</sup>*Rudolf Peierls Centre for Theoretical Physics, University of Oxford, Parks Road, Oxford OX1 3PU, United Kingdom*

 (Received 7 November 2023; revised 15 September 2024; accepted 7 November 2024; published 21 January 2025)

Decoherence is a major obstacle to the preparation of topological order in noisy intermediate-scale quantum devices. Here, we show that decoherence can also give rise to new types of topological order. Specifically, we construct concrete examples by proliferating fermionic anyons in the toric code via local quantum channels. The resulting mixed states retain long-range entanglement, which manifests in the nonzero topological entanglement negativity, though the topological quantum memory is destroyed by decoherence. By comparison with the gapless spin liquid in pure states, we show that the identified states represent a novel intrinsic mixed-state topological order, which has no counterpart in pure states. Through the lens of quantum anomalies of 1-form symmetries, we then provide general constructions of intrinsic mixed-state topological order and reveal the existence of nonbosonic deconfined anyons as another key feature of these novel phases. The extended meaning and characterization of deconfined excitations and their statistics in mixed states are clarified. Moreover, when these deconfined anyons have nontrivial braiding statistics, we prove that the mixed states cannot be prepared via finite-depth local quantum channels from any bipartite separable states. We further demonstrate our construction using the decohered Kitaev honeycomb model and the decohered double-semion model. In the latter case, a surprising scenario arises where decoherence gives rise to additional types of deconfined anyons.

DOI: [10.1103/PRXQuantum.6.010314](https://doi.org/10.1103/PRXQuantum.6.010314)

## I. INTRODUCTION

As long-range entangled (LRE) quantum matter, topologically ordered phases have attracted extensive attention in the past few decades [1–6]. Recently, there have been a growing number of theoretical proposals [7–15] as well as experimental evidence [16–21] showing that topological order (TO) can be prepared in current many-body quantum simulation platforms, such as superconducting-qubit arrays, Rydberg-atom arrays, trapped-ion systems, etc. A key feature of these noisy intermediate-scale quantum (NISQ) devices is the inevitable presence of decoherence, which renders the quantum state a mixed state [22]. Substantial progress has been made in diagnosing nontrivial topological phases subject to decoherence [23–40]. In particular, the decoherence-induced breakdown of topological

quantum memory in the toric code model is investigated and is related to the transition in the mixed-state topological order [31,33]. The topological order therein is inherited from the pure-state counterpart, which is resistant to modest decoherence. Above a certain critical error rate, the long-range entanglement is destroyed.

We are interested in the following question: Other than destroying the pure-state topological order, can decoherence give rise to novel types of topological order that are intrinsically mixed? The possibility of such an intriguing scenario arises from new mechanisms of anyon proliferation provided by decoherence, distinct from anyon condensation in pure states [41–43]. As a starting point, we explore such a possibility in the context of  $\mathbb{Z}_2$  (toric code) topological order, which comprises three types of anyon excitations,  $e$ ,  $m$ , and  $f = e \times m$ , [44–51]. In pure states, either  $e$  or  $m$  (both being self-bosons) can condense, leading to a topologically trivial Higgs/confined phase [52]. Correspondingly, proliferation of  $e$  and  $m$  anyons induced by decoherence also destroys long-range entanglement. In contrast,  $f$  anyons are self-fermions, and therefore they cannot condense in a pure state; instead, a strong fluctuation of  $f$  anyons typically leads to a gapless spin liquid, which remains LRE. This motivates us to study the fate of  $\mathbb{Z}_2$  topological order when  $f$  anyons proliferate under decoherence.

\*Contact author: wangzhongemail@tsinghua.edu.cn

†These authors contributed equally to this work.

*Published by the American Physical Society under the terms of the Creative Commons Attribution 4.0 International license. Further distribution of this work must maintain attribution to the author(s) and the published article's title, journal citation, and DOI.*

Specifically, we study the behavior of the toric code model [51] under local quantum channels that solely create  $f$  anyons. The topological quantum memory degrades to classical memory above a certain decoherence threshold, aligning with previous studies. However, it turns out that the mixed state still possesses nontrivial quantum topological order even in the absence of quantum memory. To diagnose the mixed-state topological order, we employ the topological entanglement negativity (TEN) [53–56], which is a natural generalization of the topological entanglement entropy (TEE) [57,58]. The TEN has been utilized to probe topological order in thermal equilibrium [59–62] or under shallow-depth noise channels [31], effectively acting as a faithful indicator of topological quantum memory in those studied cases. However, we find that the TEN fails to reflect topological quantum memory in this scenario and remains unchanged across the transition. Nevertheless, the nonzero TEN still points to the persistence of long-range entanglement, a hallmark of topological order. Moreover, the absence of topological quantum memory indicates that the identified topological order has no pure-state counterpart and, therefore, is termed “intrinsic mixed-state topological order” here.

We then provide further understanding of this peculiar result from the perspective of quantum anomalies. Crucially, the noisy channel proliferating  $f$  anyons preserves an anomalous 1-form symmetry generated by  $f$  anyons [63–65]. Through the anomalous 1-form symmetry, we show that the intrinsic mixed-state TO in the decohered toric code supports deconfined fermionic anyons, with a detailed explanation of the extended meaning of deconfinement and fermionic statistics in mixed states. We generally prove that mixed states with anomalous 1-form symmetries must be LRE. Moreover, we show that when the anomalous 1-form symmetry is generated by anyons with nontrivial braiding statistics, any two complementary parts of the mixed state are LRE (for arbitrary bipartition), generalizing the conjecture “mixed-state anomaly  $\Rightarrow$  multipartite nonseparability” in Ref. [66], which focuses on 0-form symmetries. With this perspective, our construction can be generalized to obtain other intrinsic mixed-state TOs, characterized by deconfined anyons with nontrivial statistics. We note that Secs. III and IV B have been added after the initial version of our work appeared on arXiv. Meanwhile, Refs. [67,68] appeared, which study the mixed-state TO from the perspective of anomalous 1-form symmetries. The discussion regarding the nonmodular-anyon theory in Sec. IV B is inspired by these works.

After introducing the general construction, we give two more examples of intrinsic mixed-state TOs, the decohered Kitaev honeycomb model and the decohered double-semion model. In the latter example, we find more surprising features in mixed-state TO. In addition to peeling off anyons in the original TO, decoherence can even

give birth to new types of deconfined anyons, which leads to a nonmodular anyon theory in our case.

The rest of the paper is organized as follows. In Sec. II, we construct an intrinsic mixed-state TO by proliferating  $f$  anyons in the toric code and reveal its properties through investigations of information quantities, including the coherent information and the TEN. We also discuss similarities and disparities to the gapless spin liquid phase in pure states. In Sec. III, we discuss general aspects of intrinsic mixed-state from the perspective of 1-form symmetry anomalies and deconfined excitations. In Sec. IV, we generalize our construction of mixed-state quantum TO to the decohered Kitaev honeycomb model and the decohered double-semion model. We conclude with a discussion in Sec. V.

## II. DECOHERED TORIC CODE AS INTRINSIC MIXED-STATE TO

### A. The model

We start with the two dimensional (2D)  $\mathbb{Z}_2$  toric code model on a square lattice:

$$H_{\text{TC}} = - \sum_v A_v - \sum_p B_p, \quad A_v \equiv \prod_{i \in v} X_i, \quad B_p \equiv \prod_{i \in p} Z_i,$$

where  $X_i$  and  $Z_i$  are Pauli matrices. The ground states are fourfold degenerate and can be used to encode two logical qubits, amenable to fault-tolerant quantum information processing. The tolerance of the topological quantum memory against local phase errors and bit-flip errors has been investigated in Refs. [23,31,33], where errors are modeled as local quantum channels,  $\mathcal{N}^z$  and  $\mathcal{N}^x$ ,

$$\mathcal{N}^x = \prod_i \mathcal{N}_i^x, \mathcal{N}_i^x[\cdot] \equiv (1 - p_x) \cdot + p_x X_i \cdot X_i, \quad (1)$$

$$\mathcal{N}^z = \prod_i \mathcal{N}_i^z, \mathcal{N}_i^z[\cdot] \equiv (1 - p_z) \cdot + p_z Z_i \cdot Z_i.$$

$p_x$  and  $p_z$  are the error rates of bit-flip and phase errors, respectively. Since these channels incoherently create  $e$  and  $m$  anyons, respectively, we denote the corresponding error-corrupted states as  $\rho_e$  and  $\rho_m$ . It has been shown that above the error threshold, the proliferation of either bosonic anyon ( $e$  or  $m$ ) would degrade the quantum memory to classical memory, accompanied by a sudden drop of the TEN from  $\log 2$  to 0. This motivates us to investigate the incoherent proliferation of the fermionic  $f$  anyons of the  $\mathbb{Z}_2$  topological order, which can be realized by the following two-qubit quantum channel:

$$\mathcal{N}^f = \prod_i \mathcal{N}_i^f, \mathcal{N}_i^f[\cdot] := (1 - p_f) \cdot + p_f Z_i X_{i+\delta} \cdot X_{i+\delta} Z_i, \quad (2)$$

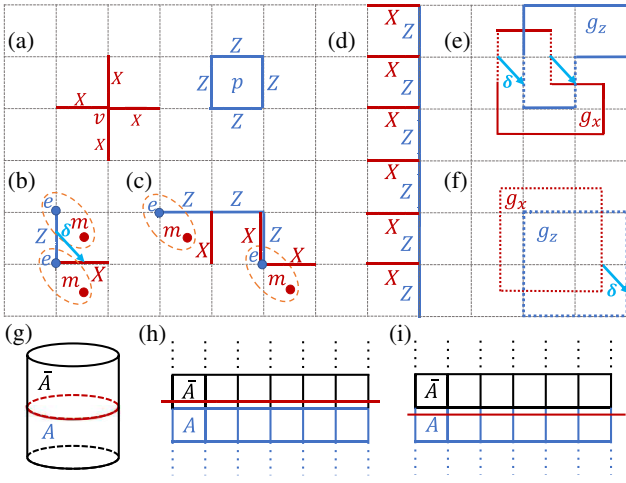


FIG. 1. (a)  $A_v$  and  $B_p$ . (b) The Kraus operator  $Z_i X_{i+\delta}$  of the quantum channel  $\mathcal{N}_i^f$  creates a pair of  $f$  anyons, labeled by orange ellipses. (c) An example of an error string  $C$  (the blue line) and  $W_C^f = \prod_{i \in C} Z_i X_{i+\delta}$ .  $f$  anyons are created at the ends of  $C$ . (d) A noncontractible-loop operator  $W_{\tilde{\gamma}_y}$  along the  $y$  direction. (e) A typical loop configuration  $g = g_x, g_z$ , with  $g_x$  colored in red and  $g_z$  in blue. The dashed (solid) lines represent segments in which  $g_x$  and  $g_z$  coincide (do not coincide)—up to a shift by  $\delta$ .  $l_g = 12$  in this example. (f) An example of a tensionless loop configuration, i.e.,  $l_g = 0$ . (g) The bipartition of a cylinder. (h),(i) Two methods of bipartition.

where  $\delta = (\frac{1}{2}, -\frac{1}{2})$  (the lattice constant is taken to be 1) and  $0 < p_f < \frac{1}{2}$  is the error rate. In this way, the ground state  $\rho_0$  is turned into a mixed state,  $\rho_f = \mathcal{N}^f[\rho_0]$ . As depicted in Fig. 1(b),  $\mathcal{N}^f$  exclusively creates  $f$  anyons. In contrast, certain other types of errors, such as the Pauli- $Y$  errors, locally create pairs of  $f$  anyons as well but globally they also produce  $e$  and  $m$  anyons, resulting in completely different outcomes. In the following sections, we demonstrate that this simple model surprisingly realizes an exotic intrinsic mixed-state topological order through analytical exact investigations of its topological memory and topological entanglement negativity.

### B. Breakdown of quantum memory

Under the  $\mathcal{N}^f$  channel, the mixed state undergoes an error-induced transition corresponding to the breakdown of quantum memory, similar to the case with bit-flip and phase errors. Such transitions can be probed by information quantities nonlinear in the density matrix, such as the coherent information  $I_c = S(\rho_f) - S(\rho_{Rf})$  [31,69,70], where  $S$  is the von Neumann entropy.  $R$  denotes reference qubits purifying the initial state  $\rho_0$ , which is taken to be the maximally mixed state in the code space,

$$\rho_0 = \frac{1}{4} \prod_v \frac{1 + A_v}{2} \prod_p \frac{1 + B_p}{2} = \text{tr}_R(|\Psi\rangle\langle\Psi|), \quad (3)$$

and  $\rho_{Rf} = \mathcal{I}_R \otimes \mathcal{N}^f[|\Psi\rangle\langle\Psi|]$  is the decohered density matrix. The coherent information measures the amount of information transmitted by the noisy channel  $\mathcal{N}$  or, in other words, it diagnoses the ability to restore the information encoded in the code space via error correction. Due to the subadditivity of the von Neumann entropy, the coherent information is bounded by  $-S(\rho_0) \leq I_c \leq S(\rho_0)$  and the sufficient and necessary condition for the existence of perfect quantum error correction is that  $I_c = S(\rho_0)$  [69]. The error threshold  $p_c$  corresponding to a sudden drop of  $I_c$  captures the breakdown of quantum memory and this error-rate threshold is an intrinsic threshold, which means that for error rate  $p > p_c$ , there is no decoding algorithm to recover the encoded quantum information.

In our model, we find that  $I_c$  can be exactly mapped to the free-energy cost of noncontractible defect lines of the random-bond Ising model (RBIM) along the Nishimori line [71], using the replica trick:

$$\begin{aligned} I_c &= -\lim_{n \rightarrow 1} \frac{\partial}{\partial n} \text{Tr}(\rho_f^n) + \lim_{n \rightarrow 1} \frac{\partial}{\partial n} \text{Tr}(\rho_{Rf}^n) \\ &= 2 \log 2 - \log \frac{\sum_{d_x, d_y=0,1} Z_{d_x, d_y}^{\text{RBIM}}}{Z_0^{\text{RBIM}}} \\ &= 2 \log 2 - \log \left[ \sum_{d_x, d_y=0,1} e^{-\Delta F_{d_x, d_y}} \right], \quad (4) \end{aligned}$$

where  $\Delta F_{d_x, d_y}$  is the excess free energy with the insertion of a noncontractible defect line and  $d_x$  and  $d_y$  count the number of noncontractible defect lines in the  $x$  and  $y$  directions, respectively. The derivation of the above mapping of  $I_c$  can be found in Appendix A 1.

For small  $p$ , the RBIM is in the ferromagnetic (FM) phase, and the excess free energy of a defect line is extensive,  $\Delta F_{\{d_x, d_y\} \neq (0,0)} \sim O(L)$ , which leads to  $I_c = 2 \log 2$ . At a critical error rate  $p_c \approx 0.109$ , the RBIM undergoes a ferromagnet-to-paramagnet phase transition, with an abrupt drop of coherent information, which determines the threshold at which the topological quantum memory is damaged beyond recovery. Nevertheless, we note that  $\rho_f$  still retains classical memory for  $p_f > p_c$ . Suppose that the initial state  $\rho_0$  is in an eigenspace of the logical operators  $W_{\tilde{\gamma}_{x,y}} = \prod_{i \in \tilde{\gamma}_{x,y}} X_i Z_{i+\delta}$ , where  $\tilde{\gamma}_x$  and  $\tilde{\gamma}_y$  are two noncontractible loops on the dual lattice. Then,  $\rho_f$  always stays in the same eigenspace under the quantum channel, as  $[W_{\tilde{\gamma}_{x,y}}, Z_i X_{i+\delta}] = 0$ .

### C. Topological entanglement negativity

Based on the above analysis, it may seem that  $\rho_f$  closely resembles  $\rho_e$  and  $\rho_m$ . However, surprisingly, we demonstrate below that even when the quantum memory breaks down for  $p_f > p_c$ ,  $\rho_f$  retains LRE with a nonzero TEN, indicating the emergence of a distinct topological order.

To evaluate the entanglement negativity of  $\rho_f$  and its scaling, we take the cylinder geometry with the bipartition  $A \cup \bar{A}$  as depicted in Fig. 1(g). Then, the logarithmic negativity is defined as

$$\varepsilon_A(\rho_f) \equiv \log \|\rho_f^{T_A}\|_1 = \varepsilon_{\bar{A}}(\rho_f), \quad (5)$$

where  $T_A$  denotes the partial transpose of  $\rho_f$  in subregion  $A$  and  $\|\cdot\|_1$  represents the trace norm. As an entanglement monotone, the logarithmic negativity is commonly used to quantify quantum entanglement in mixed states, excluding the contribution from classical correlation [72–75]. As such, it is considered a natural generalization of entanglement entropy in pure states.

For convenience, we take the initial state  $\rho_0$  to be the maximally mixed state in the code space given in Eq. (3). We denote the groups generated by  $\{A_v\}, \{B_p\}$  as  $G_{x(z)}$ :

$$G_x \equiv \langle \{A_v\} \rangle, \quad G_z \equiv \langle \{B_p\} \rangle. \quad (6)$$

Each group element  $g_{x(z)}$  corresponds to a loop configuration on the dual lattice (original lattice), as shown in Figs. 1(e) and 1(f). Thus,  $\rho_0$  can be represented by an equal-weight expansion of loop configurations:

$$\rho_0 = \frac{1}{2^N} \sum_{g_x \in G_x} \sum_{g_z \in G_z} g_x g_z = \frac{1}{2^N} \sum_{g \in G = G_x \times G_z} g. \quad (7)$$

The effect of  $\mathcal{N}^f$  is to introduce loop tension. Specifically, for a given loop  $g = g_x g_z$ ,  $\mathcal{N}^f$  assigns a weight  $1 - 2p_f$  to each segment where  $g_x$  and  $g_z$  do not coincide (up to a shift by  $\delta$ ). Consequently, we have

$$\rho_f = \mathcal{N}^f[\rho_0] = \frac{1}{2^N} \sum_{g \in G} (1 - 2p_f)^{l_g} g, \quad (8)$$

where  $l_g$  is the length of segments where  $g_x$  and  $g_z$  do not coincide. In Fig. 1(e), we illustrate how to count such segments and in Fig. 1(f), we give an example of a tensionless loop.

We now take the partial transpose for subregion  $A$ . We denote  $g = g_A g_{\bar{A}}$ , where  $g_{A(\bar{A})}$  is the restriction of operator  $g$  to subregion  $A(\bar{A})$ ,

$$\rho_f^{T_A} = \frac{1}{2^N} \sum_{g \in G} (1 - 2p_f)^{l_g} y_A(g) g, \quad (9)$$

and  $y_A(g) = 1(-1)$  when  $g_{xA}$  and  $g_{zA}$  commute (anticommute).

As shown in Figs. 1(g)–1(i), there are two possible choices of translation-invariant entanglement cut, which lead to slightly different results with regard to the TEN.

Remarkably, for the bipartition in Fig. 1(h), the final result of negativity is rather simple and is independent of  $p_f$ :

$$\varepsilon_A(\rho_f) = L \log 2 - \log 2, \quad (10)$$

where  $L$  is the length of the boundary between  $A$  and  $\bar{A}$ . For the bipartition in Fig. 1(i), however, the calculation of the negativity is much harder for general  $p_f$ . Here, we only show the results for the case with maximal decoherence,  $p_f = \frac{1}{2}$ , which is expected to reflect general features of the mixed states for  $p_f > p_c$ . In this case,  $\rho_f$  becomes the maximally mixed state, with  $W_p \equiv A_{p-\delta} B_p = 1, \forall p$ :

$$\rho_f = \frac{1}{2^{N/2+1}} \prod_p \frac{1 + W_p}{2}. \quad (11)$$

It turns out that the negativity exhibits an unusual dependence on the parity of  $L$ :

$$\varepsilon_A(\rho_f) = \begin{cases} \frac{L}{2} \log 2 - \log 2, & \text{if } L \text{ is even,} \\ \frac{L}{2} \log 2 - \frac{\log 2}{2}, & \text{if } L \text{ is odd.} \end{cases} \quad (12)$$

In all the above results, the entanglement negativity satisfies an area law and has an  $O(1)$  subleading term, known as the topological entanglement negativity, which is a generalization of the TEE. A nonzero value of the TEN signals nontrivial quantum TO, as it arises solely from long-range entanglement. For example,  $\text{TEN} = \log 2$  for the toric code ground state. Hence, it has been used to diagnose topological order in both finite-temperature systems [60] and states subject to local errors [31]. Notably, in our model, the TEN remains nonzero even if quantum memory is gone, which is in sharp contrast to the case with single-qubit  $X$  or  $Z$  errors.

The dependence of the TEN on the boundary size for the second type of bipartition seems a bit puzzling. However, this phenomenon also shows up in some ground-state topological order. Namely, the TEE or TEN also exhibits a similar even-odd dependence on the system size for  $\mathbb{Z}_2$  topological order enriched by translation symmetry through weak symmetry breaking, with typical examples including the Wen-plaquette model and the Abelian phase of the Kitaev honeycomb model [76,77]. In these cases, it is well known that the ground-state degeneracy on a torus also exhibits a similar dependence on the system size. Although there is little discussion in the literature about how weak symmetry breaking affects entanglement properties, it is straightforward to check that the subleading term of bipartite entanglement entropy on a cylinder also depends on the parity of the boundary size in these models. Based on this observation, we establish a connection between the entanglement properties of  $\rho_f$  and

ground-state  $\mathbb{Z}_2$  topological order enriched by translation symmetry in Appendix A 4.

We emphasize that the persistence of long-range entanglement signifies genuine quantum TO, which distinguishes  $\rho_f$  from the so-called classical TO, a concept raised in the study of finite-temperature TO [60,78–80]. States with classical TO have topological classical memory as well but zero TEN. One typical example is the low-temperature phase of the three-dimensional (3D) toric code model. In this sense,  $\rho_e$  and  $\rho_m$  (above the error threshold) also have classical TO.  $\rho_f$  is qualitatively different from these known examples.

#### D. Robustness of the intrinsic mixed-state TO

Although in our construction we need to use specific two-qubit channels that look a little unconventional,  $\rho_f$  represents a new type of topologically ordered phase, instead of a fine-tuned exception. We can consider the case in which single-qubit phase errors are also present:  $\rho_{f,e} = \mathcal{N}^z[\rho_f]$ , with error rate  $p_z$ . By mapping to two decoupled RBIMs, we obtain the phase diagram in Fig. 2. For small  $p_z$ ,  $\rho_{f,e}$  stays in the same phase as  $\rho_f$ , while for  $p_z > p_c \approx 0.109$ , the state undergoes another transition to the trivial phase, with no memory and zero TEN (for more details, see Appendix A 5).

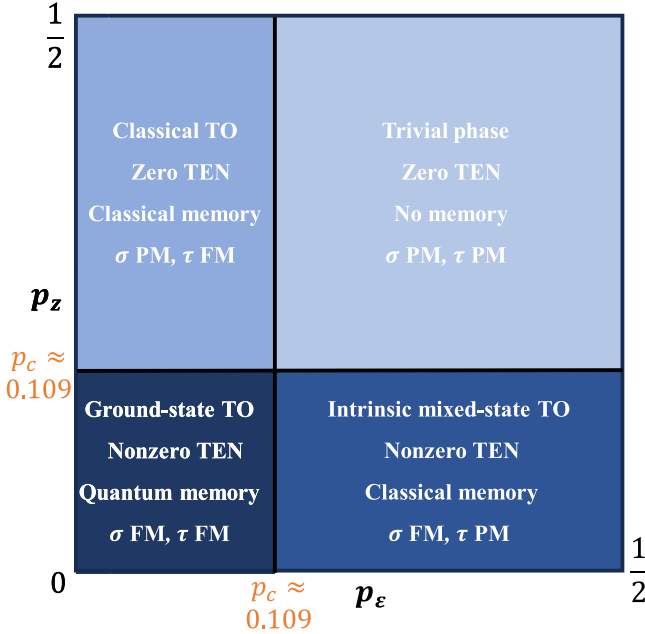


FIG. 2. The phase diagram of the toric code model subjected to both two-qubit errors and single-qubit phase errors. The properties of each phase (including topological memory and the TEN) and the corresponding phases in the two RBIMs (with Ising variables  $\sigma$  and  $\tau$ , respectively) are indicated in the phase diagram.

#### E. Comparison with anyon condensation and gapless spin liquid

From the preceding analysis, we see that although  $\rho_f$  only exhibits classical memory (for  $p_f > p_c$ ), it is fundamentally distinct from  $\rho_e$  and  $\rho_m$ . To gain deeper insight into this counterintuitive result, we draw comparisons between the error-induced anyon proliferation and anyon condensation in pure states. Instead of applying local quantum channels, we analyze the case in which the  $X_i, Z_i, Z_i X_{i+\delta}$  terms are directly introduced into the toric code Hamiltonian:

$$H = H_{\text{TC}} - \sum_i h_x X_i - h_z Z_i - h_{xz} Z_i X_{i+\delta}. \quad (13)$$

The ground-state phase diagram for  $h_{xz} = 0$  has been extensively studied [52,81–84]. For sufficiently large  $h_z$  or  $h_x$ , it leads to the condensation of  $e$  or  $m$  anyons, respectively, resulting in the destruction of long-range entanglement. Analogously, the local  $Z$  and  $X$  errors induce  $e$ - and  $m$ -anyon proliferation in an incoherent manner, which also destroys the long-range entanglement. Despite the similarities between decoherence-induced anyon proliferation and anyon condensation, there are still noteworthy distinctions. In mixed states, incoherent proliferation of either  $e$  or  $m$  does not completely trivialize the phase but, rather, leads to classical TO. Contrarily, in pure states, condensation of either  $e$  or  $m$  already leads to the trivial Higgs or confined phase.

The distinction becomes much more significant for  $f$  anyons. As fermions, they cannot condense in pure states. Then what happens when we turn on fluctuations of  $f$  anyons ( $h_{zx} \neq 0$ )? Surprisingly, at  $h_z = h_x = 0$ , this model can be exactly solved via fermionization [85]. As we show in Appendix B, when  $h_{xz}$  is sufficiently large ( $h_{x,z} = 0$ ), corresponding to large fluctuations of  $f$  particles, the system enters a gapless spin liquid phase, where  $f$  particles form a  $p$ -wave superconductor with conic dispersion, similar to the gapless Kitaev spin liquid [77]. The intrinsic mixed-state TO proposed in this paper has many features in common with the gapless spin liquid. First, they are both obtained by proliferating  $f$  anyons in the  $\mathbb{Z}_2$  TO and, as a result, neither of them has quantum memory. For the gapless spin liquid, this is due to the absence of a spectrum gap, so there is no well-defined topological degeneracy. Second, despite the lack of quantum memory, they are both LRE and are thus nontrivial phases of matter. In Sec. III, we will uncover a deeper reason for their LRE nature from the perspective of anomalies. However, there are also notable differences between  $\rho_f$  and the gapless spin liquid phase. Gapless phases typically exhibit critical forms of behavior, including algebraically decaying correlation functions and subleading logarithmic corner contributions to entanglement entropy or negativity [86–88]. Contrarily, since  $\rho_f$  is obtained by applying local quantum channels

TABLE I. A comparison between the gapless spin liquid and the intrinsic mixed-state TO ( $\rho_f$ ). For the properties listed in the last two rows, see Sec. III.

	Gapless spin liquid	Intrinsic mixed-state TO
Quantum memory	×	×
Long-range entanglement	✓	✓
Correlation of local operators	Power-law correlation	Short-range correlation
Anomalous 1-form symmetry	✓	✓
Deconfined fermions	✓	✓

on a gapped topological order, no power-law correlation can be generated, i.e.,  $\rho_f$  exhibits short-range correlation for all local operators, which is a prerequisite for any topological order. Moreover, as we have seen, the subleading term in the entanglement negativity  $\varepsilon_A(\rho_f)$  is always  $O(1)$  for  $\rho_f$ . In this sense,  $\rho_f$  also retains certain essential properties of gapped topological order. Therefore,  $\rho_f$  indeed represents a new type of topological order that is only possible in mixed states. The similarities and differences between gapless spin liquid and intrinsic mixed-state TOs are summarized in Table I.

### III. GENERALITIES: ANOMALOUS 1-FORM SYMMETRY, NONTRIVIAL STATISTICS, AND LONG-RANGE ENTANGLEMENT

The long-range entanglement of the gapless spin liquid and the intrinsic mixed-state TO are both related to an anomalous 1-form symmetry, which is generated by the following loop operators:

$$W_{\tilde{\gamma}}^f = \prod_{i \in \tilde{\gamma}} X_i Z_{i+\delta}, \quad (14)$$

where  $\tilde{\gamma}$  denotes an arbitrary loop on the dual lattice [63,64]. For noncontractible loops  $\tilde{\gamma} = \tilde{\gamma}_{x,y}$ ,  $W_{\tilde{\gamma}}^f$  are the logical operators responsible for the classical memory of  $\rho_f$  [see Fig. 1(d)]. These loop operators generate a symmetry of both models because  $[W_{\tilde{\gamma}}^f, H_{\text{TC}}] = [W_{\tilde{\gamma}}^f, Z_i X_{i+\delta}] = 0$ . In particular, we have  $W_{\tilde{\gamma}}^f \rho_f = \rho_f$  [89], which is known as the strong-symmetry condition for the mixed state [28,34,90,91]. For an open string  $\tilde{C}$ ,  $W_{\tilde{C}}^f = \prod_{i \in \tilde{C}} X_i Z_{i+\delta}$  creates two  $f$  anyons at the ends of the string, so they are referred to as  $f$  strings and the 1-form symmetry is said to be generated by  $f$  anyons. The nontrivial statistics of  $f$  anyons indicate an anomaly of the 1-form symmetry [64]. We show below that, as a consequence of the anomalous strong 1-form symmetry, the mixed state  $\rho_f$  still has deconfined fermionic excitations.

The above statement might be confusing at first sight. Since the  $f$  anyons already proliferate in  $\rho_f$ , what, then, are the deconfined fermions? Perhaps the easiest way to resolve this apparent paradox is to vectorize  $\rho$  in the double Hilbert space:  $\rho = \sum_{mn} \rho_{mn} |m\rangle\langle n| \rightarrow |\rho\rangle\rangle = \sum_{mn} \rho_{mn} |m\rangle_+ \otimes |n\rangle_-$ . For concreteness, we choose the basis  $\{|m\rangle\}$  as the eigenstates of  $Z_i$ . Then,  $|\rho_0\rangle\rangle$  corresponds to two copies of toric code ground states, with superselection sectors  $\{1, e_+, m_+, f_+\} \times \{1, e_-, m_-, f_-\}$ . The incoherent proliferation of  $f$  corresponds to condensation of  $f_+ f_-$  in this picture, which leaves  $f_+$  as a deconfined excitation, though it should now be identified with  $f_-$  due to the condensation of  $f_+ f_-$  [32]. Do these  $f_+$  anyons correspond to physical excitation in the original Hilbert space? Although the naive way to create  $f_+$  anyons  $\rho_f \rightarrow W_{\tilde{C}}^f \rho$  is not a legitimate physical process, they can be created using the unitary process  $\rho_f \rightarrow \rho'_f = U_{\tilde{C}} \rho_f U_{\tilde{C}}^\dagger$ , with  $U_{\tilde{C}} = (I + iW_{\tilde{C}}^f)/\sqrt{2}$ . Then,  $f_{+/-}$  anyons appear in the interference terms. In this sense,  $f$  anyons (we omit the “+” hereafter) remain physically meaningful excitations.

We now address another subtle question: What does “deconfinement” really mean in mixed states under noisy channels? Conventionally, it means that the energy cost does not grow indefinitely by separating individual topological excitations far apart. Here, this definition does not make sense, because the system is no longer governed by a Hamiltonian. Therefore, we propose the following definition of deconfined excitations for generic mixed states.

*Definition 1.* Given a density matrix  $\rho$ , a pair of deconfined excitations are said to be created at locations  $i$  and  $j$  in the unitary process  $\rho \rightarrow U \rho U^\dagger$  if and only if the following two conditions are satisfied:

- (1) The excitations cannot be created locally and individually. In other words,  $U$  cannot be any unitary operator supported near  $i$  and  $j$ . Typically,  $U$  is supported on an open string with endpoints  $i$  and  $j$ .
- (2) For any local operator  $O$  the support of which is away from  $i$  and  $j$ ,  $\text{tr}(\rho O) = \text{tr}(U \rho U^\dagger O)$ . This means that the change can only be detected near  $i$  and  $j$ .

Clearly, the above definition is consistent with the conventional notion of deconfined excitations and serves as a faithful and natural generalization to open quantum systems. Next, we illustrate that  $f$  anyons (we omit the “+” hereafter) are indeed deconfined excitations according to this definition, created by the unitary operator  $U_{\tilde{C}}$ . The second condition can easily be verified using the strong 1-form symmetry. We denote the support of  $O$  as  $\Omega(O)$  for convenience, which we assume to be away from  $i$  and  $j$ . If  $\Omega(O) \cap \tilde{C} = \emptyset$ , then  $\text{tr}(U_{\tilde{C}} \rho U_{\tilde{C}}^\dagger O) =$

$\text{tr}(\rho U_C^\dagger O U_C) = \text{tr}(\rho O)$ ; if  $\Omega(O) \cap \tilde{C} \neq \emptyset$ , we can always find another open string  $\tilde{C}'$ , such that  $\tilde{C} \cup \tilde{C}'$  is a contractible loop and  $\Omega(O) \cap \tilde{C}' = \emptyset$ . Using the strong 1-form symmetry  $U_{\tilde{C}'}^\dagger U_{\tilde{C}'} \rho_f = \rho_f$ , it is straightforward to obtain  $\text{tr}(U_{\tilde{C}'} \rho U_C^\dagger O) = \text{tr}(U_{\tilde{C}'} \rho U_C^\dagger O) = \text{tr}(\rho O)$ . The first condition follows from the fermionic statistics of the  $f$  anyons [92] (for more details, see also the proof of Theorem 1).

Are the fermionic statistics well defined for mixed states? We give an affirmative answer with the following microscopic method of detection (for an illustration, see Fig. 3): (a) create two  $f$  anyons at locations  $i$  and  $j$  using  $W_{ji}^f = W_{jk}^f W_{ki}^f$ ; (b) move the  $f$  anyon at  $i$  to location  $l$  using  $W_{li}^f = W_{lk}^f W_{ki}^f$ ; (c) move the other  $f$  anyon from  $j$  to  $i$  using  $W_{ij}^f = W_{ji}^{f\dagger}$ ; (d) move the  $f$  anyon at  $l$  to location  $j$  using  $W_{jl}^f = W_{jk}^f W_{kl}^f$ ; (e) annihilate the two  $f$  anyons using  $W_{ij}^f$ . In steps (b)–(d), the locations of the two  $f$  anyons are exchanged, which results in a phase  $W_{jl}^f W_{ij}^f W_{li}^f = \theta(f) = -1$ . To turn this statistical phase into an observable effect, we can use the same protocol as in Ref. [17]. That is, we introduce an ancilla qubit and prepare the initial state  $|+\rangle\langle+| \otimes \rho_f$ , where  $|+\rangle \equiv (|0\rangle + |1\rangle)/\sqrt{2}$ . Then we can use the ancilla qubit to control the exchange process. Namely, we perform steps (a)–(e) when the ancilla is in state  $|1\rangle$  and do nothing otherwise. This controlled process can be performed using the unitary operator  $V = |0\rangle\langle 0| \otimes I + |1\rangle\langle 1| \otimes W_{ij}^f W_{jl}^f W_{ij}^f W_{li}^f W_{ji}^f$ . Then, the statistical phase will manifest as the rotation of the ancilla:

$$V(|+\rangle\langle+| \otimes \rho_f) V^\dagger = |-\rangle\langle-| \otimes \rho_f, \quad (15)$$

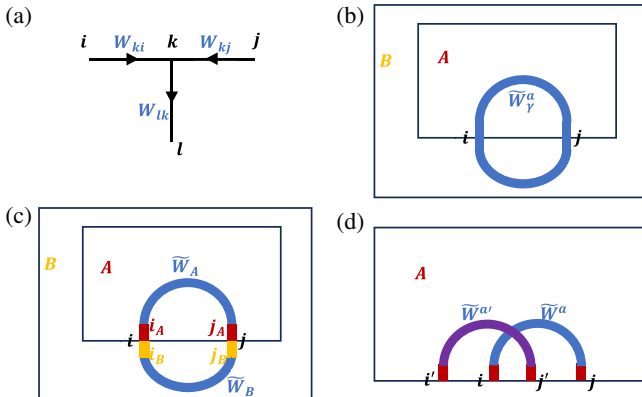


FIG. 3. (a) The exchange statistics of identical Abelian anyons can be defined using the open anyon strings  $W_{ki}, W_{kj}, W_{lk}$ . In defining open anyon strings, we require that two short strings can combine into a longer string:  $W_{i_3 i_2} W_{i_2 i_1} = W_{i_3 i_1}$ . (b) A closed  $a$  string that intersects  $\partial A$  at  $i$  and  $j$ . (c) The partitioning of  $W_\gamma^a$  into three parts: the open string  $W_{i_A j_A}^a$  and  $W_{j_B i_B}^a$  supported completely on regions  $A$  and  $B$  and the middle red and orange segments  $W_{AB}^a$  straddling between  $A$  and  $B$ . (d) The anyon strings of  $a$  and  $a'$ .

where  $|-\rangle = (|0\rangle - |1\rangle)/\sqrt{2}$ . The fermionic statistics of emergent deconfined excitations are the most striking observable effect of the intrinsic mixed-state TO. Here, they are guaranteed by the anomalous strong 1-form symmetry.

In the double space,  $e_+ e_-$  also remains a deconfined excitation, which has mutual semion statistics with  $f_+$ . Surprisingly, these braiding statistics can also be (partially) detected in the physical Hilbert space, as we demonstrate below. First, note that  $\rho_f$  preserves a weak 1-form symmetry generated by  $e$  anyons,  $W_\gamma^e \rho_f W_\gamma^e = \rho$  for a contractible closed  $e$  string  $W_\gamma^e$  [28]. Then, based on Definition 1, deconfined excitations can be created using an open  $e$  string,  $\rho_f \rightarrow \rho_f^e = W_C^e \rho_f W_C^e$ . Second, introduce an ancilla qubit and prepare the initial state  $|+\rangle\langle+| \otimes \rho_f^e$ . Then use the ancilla qubit to control the braiding process: if the ancilla is in  $|1\rangle$ , we create two  $f$  anyons and drag one of them along a loop  $l$  enclosing the  $e$  anyon, and finally annihilate with the other  $f$  anyon, as illustrated in Fig. 4; if the ancilla is in  $|0\rangle$ , we do nothing. This controlled process can be performed using the unitary gate  $V = |0\rangle\langle 0| \otimes I + |1\rangle\langle 1| \otimes W_\gamma^f$ , where  $W_\gamma^f = \prod_{i \in \text{loop } \gamma} X_i Z_{i+\delta}$ . Then, the braiding statistics can be detected by rotation of the ancilla qubit:

$$V(|+\rangle\langle+| \otimes \rho_f^e) V^\dagger = |-\rangle\langle-| \otimes \rho_f^e. \quad (16)$$

Stated more formally, the braiding statistics reflect the mixed anomaly between the weak 1-form symmetry (generated by  $e$ ) and the strong 1-form symmetry (generated by  $f$ ) [93].

One key distinction compared to the usual anyon braiding is that the  $f$ - $e$  braiding here is only one-way defined under the above protocol. Namely, the statistical phase can only be detected by moving  $f$  around  $e$  (with the movement of  $f$  controlled by the ancilla) but not the other way around [94]. This directly follows from the fact that while  $f$  anyons generate a strong 1-form symmetry,  $e$  anyons only generate a weak 1-form symmetry. Therefore, a finer characterization of deconfined excitations than Definition 1 is needed and we call the former type strongly deconfined and the latter type weakly deconfined. As demonstrated above, strongly deconfined anyons are allowed to form coherent superposition states and their statistics can be detected from the interference effects. Weakly deconfined anyons, on the other hand, always have trivial exchange and braiding statistics among themselves and can have one-way braiding statistics with strongly deconfined anyons. In the rest of the paper, we mainly focus on strongly deconfined anyons.

Using the perspective of anomalies, we can generalize our construction to obtain other intrinsic mixed-state TOs [67,68]. Given a TO with anyon content  $\mathcal{A}$ , one can incoherently proliferate a subset  $\mathcal{B} \subset \mathcal{A}$  of anyons using a

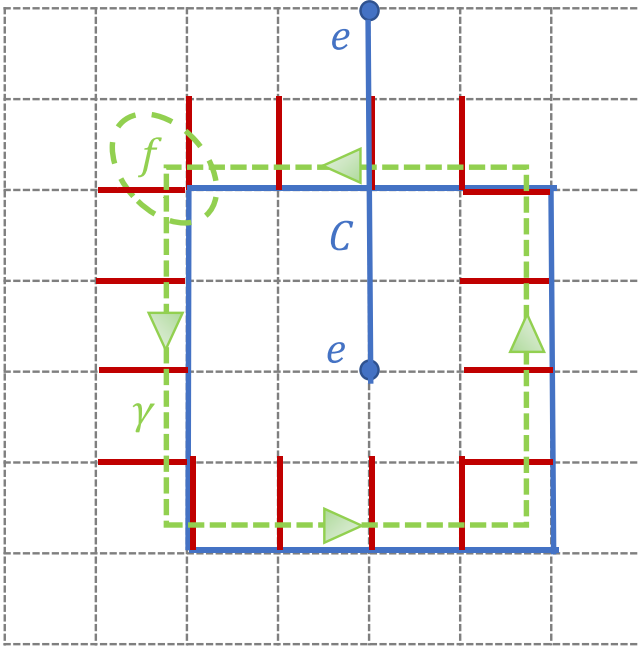


FIG. 4. Braiding between  $f$  and  $e$ . The quantum channel  $\mathcal{N}^f$  does not affect the braiding statistics, because it preserves the weak 1-form symmetry generated by  $e$  and the strong 1-form symmetry generated by  $f$ .

noisy channel, taking the Kraus operator to be the shortest string of anyons in  $\mathcal{B}$ . If there exists some Abelian anyon  $a \in \mathcal{A}$  that has trivial braiding with all anyons in  $\mathcal{B}$ , then closed  $a$  strings commute with the Kraus operators. Therefore, the  $a$  anyons generate a strong 1-form symmetry [95]. Based on the previous discussion, this means that they remain deconfined excitations with well-defined statistics. When they have nontrivial statistics,  $\theta(a) \neq 1$ , then the 1-form symmetry is anomalous. For example, in the model discussed above,  $\mathcal{A} = \{1, e, m, f\}$ ,  $\mathcal{B} = \{f\}$ , and  $a = f$  because fermions have trivial full braiding with themselves.

The existence of nonbosonic strongly deconfined excitation can be viewed as another diagnosis of nontrivial mixed-state TOs, complementary to the TEN. Indeed, we show below that this property generically implies the mixed state to be LRE, without explicit calculation of negativity.

*Theorem 1.* Consider a 2D state  $\rho$  with anomalous strong 1-form symmetry generated by some Abelian anyon  $a$  with  $\theta(a) \neq 1$ , i.e.,  $W_\gamma^a \rho = \rho$ , where the  $W_\gamma^a$  are closed  $a$  strings supported on any contractible loop  $\gamma$ . Then,  $\rho$  cannot be prepared using a finite-depth local channel (FDLC) from any fully separable state:

$$\rho \neq \mathcal{N}_{\text{FDLC}} \left[ \sum_{\lambda} p_{\lambda} \bigotimes_{\text{site } i} |\psi_i^{\lambda}\rangle \langle \psi_i^{\lambda}| \right] \quad (p_{\lambda} > 0). \quad (17)$$

Before the proof, we give some remarks regarding the above theorem.

- (1) Following Refs. [96,97], Eq. (17) can be viewed as the definition of long-range entanglement for generic mixed states. Thus the above theorem tells us that anomalous strong 1-form symmetries must lead to nontrivial mixed-state quantum TOs.
- (2) Typically, the 1-form symmetry includes generators supported on noncontractible loops. However, here we only require the symmetry condition for contractible ones, enabling a much wider range of applications. For example, for the construction of intrinsic mixed-state TOs discussed above, the pre-decoherence state can be taken to be any state in the ground-state subspace. The above theorem can also be applied to topologically trivial spatial manifolds such as a 2-sphere.
- (3) Similar to the discussion before Eq. (15), the anomaly manifests as the algebra of open-string operators:

$$\begin{aligned} W_{i_3 i_2}^a W_{i_2 i_1}^a &= W_{i_3 i_1}^a, W_{i_1 i_2}^\dagger = W_{i_2 i_1}, \\ W_{k_j}^a W_{l_k}^a W_{k_m}^a &= \theta(a) W_{k_m}^a W_{l_k}^a W_{k_j}^a. \end{aligned} \quad (18)$$

Essentially, the nontrivial statistics  $\theta(a) \neq 1$  of  $a$  are all we need in the following proof.

- (4) Notably, the condition that we impose automatically includes the case of a mixed anomaly between strong 1-form symmetries, which arises when two strongly deconfined Abelian anyons  $a$  and  $a'$  have nontrivial mutual statistics,  $B_\theta(a, a') \neq 1$  ( $B_\theta(a, a')$  is the statistical phase from a full braiding between  $a$  and  $a'$ ). Using the relation  $B_\theta(a, a') = \theta(aa')/(\theta(a)\theta(a'))$ , the mixed anomaly implies that at least one of  $a$ ,  $a'$ , and  $aa'$  has nontrivial self-statistics  $\theta \neq 1$ . Thus we do not need to consider mutual statistics separately.
- (5) To prove the theorem, we make an additional assumption that  $W_\gamma^a$  can be expressed using a finite-depth local unitary circuit (FDLUC), which is usually the case for Abelian anyon  $a$ .

*Proof.* Suppose, by contradiction, that  $\rho = \mathcal{N}_{\text{FDLC}}[\sum_{\lambda} p_{\lambda} \bigotimes_{\text{site } i} |\psi_i^{\lambda}\rangle \langle \psi_i^{\lambda}|]$ . Recall that a generic FDLUC  $\mathcal{N}$  can be constructed in three steps: first, introduce auxiliary degrees of freedom on each site; second, apply an FDLUC on the system and the auxiliary degrees of freedom; and third, trace out the added degrees of freedom. This can be written as  $\mathcal{N}_{\text{FDLC}}[\rho_0] = \text{tr}_E[U_{SE} \rho_0 \bigotimes_{\text{site } i} |e_i\rangle \langle e_i| U_{SE}^\dagger]$ , where  $U_{SE}$  is a FDLUC. If  $\rho_0$  is a fully separable state, then  $\rho = \mathcal{N}_{\text{FDLC}}[\rho_0]$  is of the form  $\rho = \sum_{\lambda} p_{\lambda} \text{tr}_E[U_{SE} \bigotimes_i |\phi_i\rangle \langle \phi_i| U_{SE}^\dagger]$ , where  $|\phi_i\rangle \equiv |\psi_i^{\lambda}\rangle \otimes |e_i\rangle$ . Then, each pure state  $U_{SE} \bigotimes_i |\phi_i\rangle$  must be symmetric:  $W_\gamma^a U_{SE} \bigotimes_i |\phi_i\rangle =$



$U_{SE} \otimes_i |\phi_i\rangle$ . Equivalently,  $\tilde{W}_\gamma^a = U_{SE}^\dagger W_\gamma^a U_{SE}$  is a symmetry of the product state  $\otimes_i |\phi_i\rangle$ . Crucially, the restriction of  $\tilde{W}^a$  to open strings  $\tilde{W}_{i_1 i_2}^a \equiv U_{SE}^\dagger W_{i_1 i_2}^a U_{SE}$  satisfies the same algebra, given in Eq. (18), as  $W^a$ . As we show below, this will lead to a contradiction.

Since any contractible-loop operator  $\tilde{W}_\gamma^a$  is a symmetry, an open string  $\tilde{W}_{i_1 i_2}^a$  can only change the state near the end of the string:  $\tilde{W}_{i_1 i_2}^a \otimes_i |\phi_i\rangle = A_{i_1} B_{i_2} \otimes_i |\phi_i\rangle$ , where  $A_{i_1}$  and  $B_{i_2}$  are unitary operators supported near  $i_1$  and  $i_2$ , respectively. From the algebraic relation given in Eq. (18),

$$\tilde{W}_{kj}^a \tilde{W}_{lm}^a = \theta(a) \tilde{W}_{km}^a \tilde{W}_{lj}^a. \quad (19)$$

By applying both sides of the equation to  $\otimes_i |\phi_i\rangle$ , we obtain  $A_k \otimes B_j \otimes A_l \otimes B_m \otimes_i |\phi_i\rangle = \theta(a) A_k \otimes B_m \otimes A_l \otimes B_j \otimes_i |\phi_i\rangle$ , which leads to a contradiction when  $\theta(a) \neq 1$ . ■

The above proof shows that nontrivial TOs are guaranteed by the existence of nonbosonic deconfined excitation  $a$ , even for mixed states. Furthermore, when  $a$  is neither bosonic nor fermionic,  $\theta(a) \neq \pm 1$ , or when  $a$  has nontrivial mutual statistics with another strongly deconfined anyon  $a'$ , then an even stronger conclusion can be proved.

*Theorem 2.* Consider a 2D state  $\rho$  with an anomalous strong 1-form symmetry generated by Abelian anyons  $a$  and  $a'$ , with nontrivial braiding statistics  $B_\theta(a, a') \neq 1$  (with the special case  $a = a'$  included). Then, for any bipartition  $A \cup B$  with linear size  $L_A, L_B \rightarrow \infty$  in the thermodynamic limit,  $\rho$  cannot be prepared using an FDL from any bipartite separable state:

$$\rho \neq \mathcal{N}_{\text{FDLC}} \left[ \sum_\lambda p_\lambda |\psi_A^\lambda\rangle \langle \psi_A^\lambda| \otimes |\psi_B^\lambda\rangle \langle \psi_B^\lambda| \right]. \quad (20)$$

Again, we only need the symmetry condition  $W_\gamma^a \rho = \rho, W_\gamma^{a'} \rho = \rho$  for contractible-loop operators  $W_\gamma^a, W_\gamma^{a'}$ , which we assume to be FDLUCs.

*Proof.* Suppose, by contradiction, that  $\rho = \mathcal{N}_{\text{FDLC}} \left[ \sum_\lambda p_\lambda |\psi_A^\lambda\rangle \langle \psi_A^\lambda| \otimes |\psi_B^\lambda\rangle \langle \psi_B^\lambda| \right]$ . Following the same steps as in the proof of Theorem 1, we have

$$\tilde{W}_\gamma^a |\phi_A\rangle \otimes |\phi_B\rangle = |\phi_A\rangle \otimes |\phi_B\rangle, \quad (21)$$

with the bipartite product state  $|\phi_A\rangle \otimes |\phi_B\rangle$  and the 1-form symmetry generator  $\tilde{W}_\gamma^a$  defined in an enlarged Hilbert space  $\mathcal{H}_S \otimes \mathcal{H}_E$ . Next, we take a loop  $\gamma$  intersecting the boundary between  $A$  and  $B$  at locations  $i$  and  $j$ , with the corresponding closed  $a$  string  $\tilde{W}_\gamma^a$ . We extract a small segment of  $\tilde{W}_\gamma^a$  near the intersection points, denoted by  $\tilde{W}_{AB}^a$ , such that  $\tilde{W}_\gamma^a$  can be written as  $\tilde{W}_\gamma^a = \tilde{W}_{iAJA}^a \tilde{W}_{jBiB}^a \tilde{W}_{AB}^a$ ,

where  $\tilde{W}_{iAJA}^a, \tilde{W}_{jBiB}^a$  are open  $a$  strings completely supported on  $A$  and  $B$ , respectively. Then, we have

$$\begin{aligned} \tilde{W}_{AB}^a |\phi_A\rangle \otimes |\phi_B\rangle &= \tilde{W}_{iAJA}^{a\dagger} |\phi_A\rangle \otimes \tilde{W}_{jBiB}^{a\dagger} |\phi_B\rangle \\ &\Rightarrow \text{tr}_{B \cup \sigma_{ij}} [|\phi_A\rangle \langle \phi_A| \otimes |\phi_B\rangle \langle \phi_B|] \\ &= \text{tr}_{B \cup \sigma_{ij}} [\tilde{W}_{iAJA}^{a\dagger} |\phi_A\rangle \langle \phi_A| \tilde{W}_{iAJA}^a \otimes |\phi_B\rangle \langle \phi_B|] \\ &\Rightarrow \text{tr}_{\sigma_{ij}} [|\phi_A\rangle \langle \phi_A|] = \text{tr}_{\sigma_{ij}} [\tilde{W}_{iAJA}^{a\dagger} |\phi_A\rangle \langle \phi_A| \tilde{W}_{iAJA}^a], \end{aligned} \quad (22)$$

where  $\sigma_{ij}$  denotes the union of the two red segments in Fig. 3(c). Due to the unitary equivalence of purification [98],

$$\begin{aligned} \exists u_{\sigma_{ij}} \text{ supported on } \sigma_{ij}, \text{ such that } u_{\sigma_{ij}} |\phi_A\rangle &= \tilde{W}_{iAJA}^{a\dagger} |\phi_A\rangle \\ \Rightarrow u_{\sigma_{ij}}^\dagger \tilde{W}_{jAJA}^a |\phi_A\rangle &= |\phi_A\rangle. \end{aligned} \quad (23)$$

Physically, this means that a pair of  $a$  and its antiparticle are created in the bulk of  $A$ , moving apart toward  $\partial A$ , and they get eliminated on the boundary (by a unitary process with local support). Below, we show that such a process contradicts the anyonic statistics of  $a$  [99,100]. Now consider the closed  $a'$  string  $W_{\gamma'}^{a'}$ , which intersects the boundary  $\partial A$  at  $i'$  and  $j'$ , with the distance between  $i, j, i',$  and  $j'$  sufficiently large compared to the depth of  $\mathcal{N}_{\text{FDLC}}$ . Similarly to the above analysis,

$$\exists u_{\sigma_{i'j'}} \text{ supported on } \sigma_{i'j'}, \text{ such that } u_{\sigma_{i'j'}}^\dagger \tilde{W}_{j'Ai'A}^{a'} |\phi_A\rangle = |\phi_A\rangle. \quad (24)$$

On the other hand, from the braiding statistics between  $a$  and  $a'$ ,

$$\begin{aligned} \tilde{W}_{j'Ai'A}^{a'} \tilde{W}_{jAJA}^a &= B_\theta(a, a') \tilde{W}_{jAJA}^a \tilde{W}_{j'Ai'A}^{a'} \\ \Rightarrow u_{\sigma_{i'j'}}^\dagger \tilde{W}_{j'Ai'A}^{a'} u_{\sigma_{ij}}^\dagger \tilde{W}_{jAJA}^a &= B_\theta(a, a') u_{\sigma_{ij}}^\dagger \tilde{W}_{jAJA}^a u_{\sigma_{i'j'}}^\dagger \tilde{W}_{j'Ai'A}^{a'}, \end{aligned} \quad (25)$$

which is inconsistent with Eqs. (23) and (24) when  $B_\theta(a, a') \neq 1$ . ■

We can restate Theorem 2 in the following way: if a mixed state has strongly deconfined Abelian anyons with nontrivial braiding statistics, then for any bipartition, there must be long-range entanglement between the two complementary regions. Notably, our discussion includes the scenario  $a' = a$ , in which case  $B_\theta(a, a') = \theta^2(a)$ . Compared to Theorem 1, we leave behind the case that  $a$  has fermionic self-statistics but trivial mutual braiding statistics with other deconfined anyons. In such cases,  $a$  also generates an anomalous strong 1-form symmetry but our proof does not work. Nevertheless, the decohered toric code under “ZX” errors that we construct is indeed bipartite LRE, indicated

by the nonzero TEN, which arguably should also be related to the anomalous strong 1-form symmetry generated by  $f$  anyons. It is intriguing to explore whether the existence of deconfined fermions also generically leads to bipartite LRE mixed states.

The above results can be viewed as a generalization of the results in Ref. [66], where it is conjectured that mixed states with anomalous strong 0-form symmetry in  $d$  spatial dimensions cannot be prepared via an FDL from any  $(d+2)$ -partite separable states. In two dimensions, this means that the mixed states cannot be prepared via an FDL from a 4-partite nonseparable state, with the additional condition that three of the four parts intersect at one point. Our results show that anomalies of 1-form symmetries can have a stronger constraining power, since bipartite nonseparability implies multipartite nonseparability but not vice versa.

#### IV. GENERALIZATIONS TO OTHER INTRINSIC MIXED-STATE TOs

##### A. Decohered Kitaev honeycomb model

In Sec. III, we have provided a general route to generalize the construction in Sec. II to obtain other intrinsic mixed-state TOs. In this section, we give two more examples as applications. We first discuss the generalization to the Kitaev honeycomb model:  $H = -J_x \sum_{x \text{ bonds}} \sigma_j^x \sigma_k^x - J_y \sum_{y \text{ bonds}} \sigma_j^y \sigma_k^y - J_z \sum_{z \text{ bonds}} \sigma_j^z \sigma_k^z - \sum_i \vec{h} \cdot \vec{\sigma}_i$  (with  $|\vec{h}| \ll |J_\mu|$ ,  $\mu = x, y, z$ ). See Fig. 5 for the definition of the three types of bonds. This model can be exactly solved by mapping it to Majorana fermions coupled to static  $\mathbb{Z}_2$

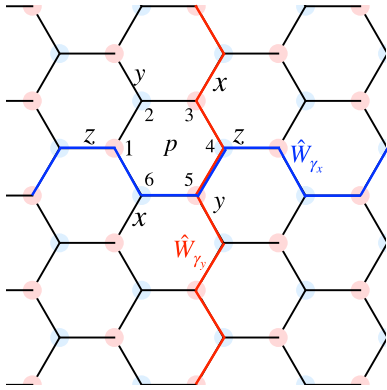


FIG. 5. The Kitaev honeycomb model, logical operators, and flux operators. All the bonds are classified into three different equivalence classes of parallel bonds:  $x$  bonds,  $y$  bonds, and  $z$  bonds. There is a two-spin interaction,  $\sigma_i^\alpha \sigma_j^\alpha$ , on each  $\alpha$  bond, where  $\alpha = x, y, z$ . The two noncontractible-loop operators  $W_{\gamma_x}$  and  $W_{\gamma_y}$ , illustrated as blue and red, are the product of the two-spin interactions on the bonds along those loops. In each plaquette  $p$ , there is a conserved flux operator  $W_p^f = \sigma_1^z \sigma_2^y \sigma_3^x \sigma_4^z \sigma_5^y \sigma_6^x$ .

gauge fields [51]. It is shown that the ground state  $\rho_0$  of this model can realize Abelian  $\mathbb{Z}_2$  TO and non-Abelian Ising TO, as well as a gapless  $\mathbb{Z}_2$  spin liquid phase. All three phases have deconfined fermion excitations.

To obtain intrinsic mixed-state TOs, we construct the following channel:

$$\rho_f = \mathcal{N}^X \circ \mathcal{N}^Y \circ \mathcal{N}^Z[\rho_0], \quad \mathcal{N}^\alpha = \prod_{(ij) \in \alpha \text{ bonds}} \mathcal{N}_{(ij)}^\alpha,$$

$$\mathcal{N}_{(ij)}^\alpha[\rho_0] = p \sigma_i^\alpha \sigma_j^\alpha \rho_0 \sigma_j^\alpha \sigma_i^\alpha + (1-p) \rho_0. \quad (26)$$

This channel leads to decoherence of the fermions but preserves the  $\mathbb{Z}_2$  gauge flux. In other words, it preserves the anomalous 1-form symmetry, with generators  $W_p^f = \sigma_1^z \sigma_2^y \sigma_3^x \sigma_4^z \sigma_5^y \sigma_6^x$  [101]. Therefore, the resulting mixed states must be LRE and must support deconfined fermionic excitations. In the maximally decohered case  $p_f = \frac{1}{2}$ , the  $f$  particles are heated to infinite temperature, so all of the three ground-state phases will end up in the maximally mixed state in the zero-flux sector ( $W_p^f = 1, \forall p$ ), which belongs to the same intrinsic mixed-state TO as that constructed in Sec. II. Actually, at  $p_f = \frac{1}{2}$ , this state can be obtained by applying a Hadamard gate on all vertical links to Eq. (11). Therefore, the decohered honeycomb model constructed here is also characterized by a nonzero TEN. We note that a similar model in the context of Lindblad equations has been constructed in Ref. [102] but that the LRE nature has not been uncovered.

##### B. Decohered double-semion model

As another example, we construct intrinsic mixed-state TOs from the double-semion TO. The anyon content of the double-semion TO is  $\mathcal{A} = \{1, s, \bar{s}, s\bar{s}\} = \{1, s\} \times \{1, \bar{s}\}$ , where  $s$  is a semion,  $\theta(s) = i$ ;  $\bar{s}$  is an antiseimion,  $\theta(\bar{s}) = -i$ ; and  $s\bar{s}$  is a boson,  $\theta(s\bar{s}) = 1$ . The fusion rules are  $s \times s = 1, \bar{s} \times \bar{s} = 1, s \times \bar{s} = s\bar{s}$  [103]. Following the general strategy in Sec. III, we can proliferate the semion  $s$  using noisy channels, and due to the trivial braiding between  $s$  and  $\bar{s}$ , the 1-form symmetry generated by  $\bar{s}$  is preserved. Thus  $\bar{s}$  remains a strongly deconfined excitation with well-defined antiseimionic statistics.

For concreteness, we start with the Pauli-stabilizer model realizing the double-semion TO [104]. The model is defined on a 2D square lattice with a  $\mathbb{Z}_4$  degree of freedom on each link, which is equipped with the Pauli operators  $Z = \sum_{n \in \mathbb{Z}_4} i^n |n\rangle \langle n|$  and  $X = \sum_{n \in \mathbb{Z}_4} |n+1\rangle \langle n|$ . The stabilizer model is defined as follows:

$$H_{\text{DS}} = - \sum_p (A_{v=p-\delta} B_p^{-1} + \text{h.c.}) - \sum_p B_p^2 - \sum_i C_i, \quad (27)$$

where  $A_v$ ,  $B_p$ , and  $C_i$  are represented graphically in Fig. 6(a). Below, we briefly review how this model is

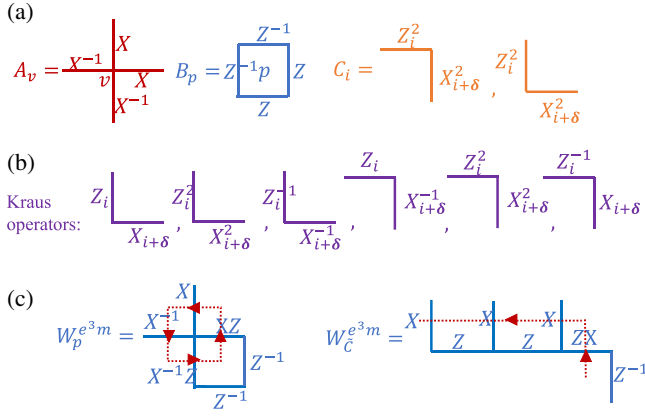


FIG. 6. (a) The stabilizers used in defining  $H_{\mathbb{Z}_4 \text{ TC}}$  and  $H_{\text{DS}}$ . (b) The Kraus operators in the decohered double-semion model. They are the shortest string operators of  $[em]$  anyons. (c) A shortest closed  $e^3 m$  string,  $W_p^{e^3 m}$ , and an open  $e^3 m$  string,  $W_C^{e^3 m}$ .

constructed from a parent  $\mathbb{Z}_4$  toric code:

$$H_{\mathbb{Z}_4 \text{ TC}} = - \sum_v A_v - \sum_p B_p + \text{h.c.} \quad (28)$$

The anyon content of the  $\mathbb{Z}_4$  toric code is  $\{e^n m^r (n, r = 0, 1, 2, 3)\}$  with a  $\mathbb{Z}_4 \times \mathbb{Z}_4$  fusion rule,  $e^4 = m^4 = 1$ . The statistics of the 16 anyons are given by  $\theta(e^n m^r) = i^{nr}$ . The double-semion TO described by  $H_{\text{DS}}$  is obtained by condensing the boson  $e^2 m^2$  in the  $\mathbb{Z}_4$  toric code (the  $C_i$  term is the shortest string operator of  $e^2 m^2$ , leading to its condensation), which causes confinement of anyons with nontrivial braiding with  $e^2 m^2$  and identification of anyons related by fusion with  $e^2 m^2$ . Namely,  $[a] = [a \times e^2 m^2]$  in the condensed theory, where we use  $[a]$  to label the remaining deconfined anyons after the  $e^2 m^2$  condensation. The deconfined anyons in the condensed theory are  $\{[1], [em], [e^3 m], [e^2]\} = \{[1], [em]\} \times \{[1], [e^3 m]\}$ , where  $[em]$  is a semion and  $[e^3 m]$  is an antisemion. Indeed, a double-semion TO is realized.

Next, we investigate the effect of proliferating  $[em]$  anyons using the following quantum channel:

$$\mathcal{N}^{[em]} = \prod_i \mathcal{N}_i^{[em]}, \mathcal{N}_i^{[em]}[\cdot] \equiv \sum_{n=0,1,2,3} p_n K_i^n \cdot K_i^{n\dagger}. \quad (29)$$

The Kraus operators  $K_i$  and  $K_i^\dagger$  are the shortest string operators of  $em$  anyons in the  $\mathbb{Z}_4$  toric code:

$$K_i = \begin{cases} Z_i X_{i+\delta} & \text{for vertical link } i, \\ Z_i X_{i+\delta}^{-1} & \text{for horizontal link } i. \end{cases} \quad (30)$$

For simplicity, we take the initial state  $\rho_0$  to be the maximally mixed state in the ground-state subspace of  $H_{\text{DS}}$  and directly consider the maximally decohered case  $p_0 = p_1 =$

$p_2 = p_3 = \frac{1}{4}$ . Based on the analysis at the beginning of this section, it seems that only the antisemion  $[e^3 m]$  will remain strongly deconfined, which leads to a chiral-antisemion theory  $\{1, [e^3 m]\}$ . However, the actual situation turns out to be even more intriguing.

First, we note that the 1-form symmetry generated by  $e^3 m$  is indeed preserved because  $[W_Y^{e^3 m}, K_i] = 0$ , for any closed  $e^3 m$  strings, which implies that  $e^3 m$  is a deconfined anyon. Examples of a shortest closed  $e^3 m$  string as well as an open  $e^3 m$  string are given in Fig. 6(c). On the other hand, the  $C_i$  terms in  $H_{\text{DS}}$  do not commute with the Kraus operators. As a result, for any open  $e^2 m^2$  string  $W_C^{e^2 m^2} = \prod_{i \in C} C_i$ ,  $\text{tr}(\rho W_C^{e^2 m^2})$  becomes 0 for  $\rho = \mathcal{N}^{[em]}[\rho_0]$ . This means that the  $e^2 m^2$  anyons are revolved from the Bose-Einstein condensate and become a detectable anyon. Notably, the  $e^2 m^2$  still proliferate classically, which is very different from Bose-Einstein condensation, as we have noted previously. Moreover, due to the strong 1-form symmetry generated by  $e^3 m$  and the fusion rule  $e^3 m \times e^3 m = e^2 m^2$ ,  $e^2 m^2$  must become a deconfined anyon. Therefore, the remaining strongly deconfined anyons in  $\rho$  form a  $\mathbb{Z}_4$  group  $\{1, e^3 m, e^2 m^2, em^3\}$ . We note that  $e^3 m$  and  $em^3$  are both antisemions and that  $e^2 m^2$  is a transparent boson, meaning that its presence cannot be remotely detected via an Aharonov-Bohm measurement, i.e., a full braid of any strongly deconfined anyon around it only results in a unity phase factor. Anyon theories with transparent bosons or fermions are known as nonmodular anyon theories [77,105]. It is widely believed that nonmodular anyon theories cannot be realized by local gapped Hamiltonians in 2D bosonic systems [100,106]. This implies the lack of a pure-state counterpart of the mixed-state TO; thus it is indeed intrinsically mixed. Notably, the intrinsic mixed-state TO constructed in Sec. II is also nonmodular, with strongly deconfined anyons  $\{1, f\}$ . One crucial difference is that here the intrinsic mixed-state TO does have a quantum memory. The undamaged part of the stored information is manipulated by the logical operators shown in Fig. 7:

$$W_{\tilde{\gamma}_x}^{e^3 m} = \prod_{i \in \tilde{\gamma}_x} X_i Z_{i+\delta}, W_{\tilde{\gamma}_y}^{e^3 m} = \prod_{i \in \tilde{\gamma}_y} X_i Z_{i+\delta}^{-1}. \quad (31)$$

$W_{\tilde{\gamma}_x}^{e^3 m} W_{\tilde{\gamma}_y}^{e^3 m} = -W_{\tilde{\gamma}_y}^{e^3 m} W_{\tilde{\gamma}_x}^{e^3 m}$  as a consequence of the nontrivial self-braiding statistics of  $e^3 m$ . Besides, both  $(W_{\tilde{\gamma}_x}^{e^3 m})^2$  and  $(W_{\tilde{\gamma}_y}^{e^3 m})^2$  are elements of the stabilizer group defined by  $H_{\text{DS}}$ , thus acting trivially in the code space. Therefore, the intrinsic mixed-state TO supports quantum memory with one and only one logical qubit. Remarkably, the anyon theory here is identical to the one obtained by incoherently proliferating the  $em$ ,  $e^2 m^2$ , and  $e^3 m^3$  in the  $\mathbb{Z}_4$  toric code via the same channel,  $\mathcal{N}^{[em]}$  [67,68]. The relation among the  $\mathbb{Z}_4$  toric code, double-semion, and nonmodular

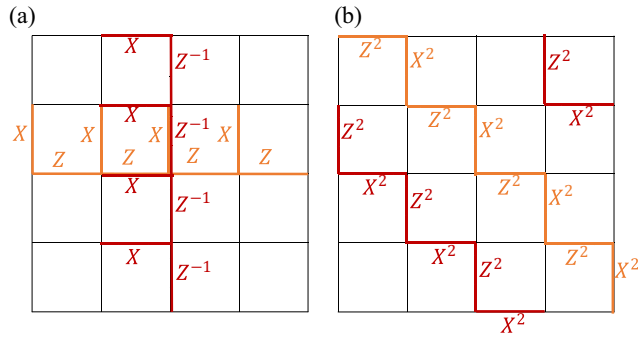


FIG. 7. (a) Two logical operators  $W_x^{e^3 m}$  (in orange) and  $W_y^{e^3 m}$  (in red). (b) Two nonlocal stabilizers. In both (a) and (b), periodic boundary conditions are imposed.

anyon theory is summarized in Fig. 8. However, it does not imply that the final mixed states in the two models are identical. Actually, the decohered  $\mathbb{Z}_4$  toric code model (under  $\mathcal{N}^{[em]}$ ) is fully characterized by the stabilizer group  $G_{e^3 m} = \langle \{W_p^{e^3 m}\} \rangle$ , which defines the code space  $\mathcal{H}_C$ :

$$\mathcal{H}_C = \{ |\psi\rangle, g|\psi\rangle = |\psi\rangle, \forall g \in G_{e^3 m} \}. \quad (32)$$

In the maximally decohered case, the final state is the maximally mixed state in  $\mathcal{H}_C$ . For the decohered double-semion model, however, there are additional nonlocal stabilizers formed by products of  $C_i$ . Two such nonlocal stabilizers are depicted in Fig. 7 and other nonlocal stabilizers can be obtained from these two via translation along the horizontal direction.

We summarize several surprising features of intrinsic mixed-state TOs revealed by this example. First, novel nonmodular TOs beyond the usual unitary modular tensor category description of 2+1D TOs can be easily realized by Pauli-stabilizer models under decoherence [67,68]. Second, decoherence can sometimes give rise to new types of deconfined anyons that are absent in the anyon theory supported by the ground-state TO. This further implies that some features of the mixed-state TO can go beyond the prediction based on the IR theory or the anyon data of the original topological order (i.e., before decoherence),

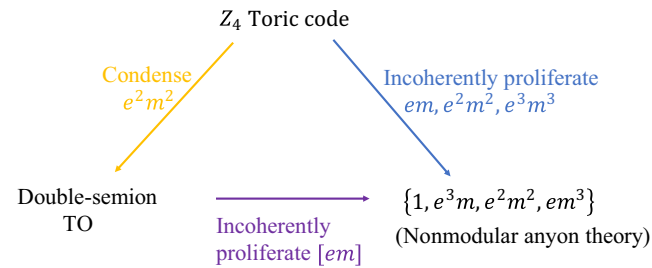


FIG. 8. The relation among the  $\mathbb{Z}_4$  toric code, the double-semion code, and the nonmodular anyon theory supported by intrinsic mixed-state TOs.

including the field-theoretic description [32,33]. Indeed, if we were to start from other lattice realizations of double-semion topological order, e.g., the  $\mathbb{Z}_4$  Pauli-stabilizer code introduced in Ref. [105] [which is a variant of Eq. (27)] or the twisted  $\mathbb{Z}_2$  lattice gauge theory in [99,107–110], and incoherently proliferate semions via quantum channels, we would obtain a chiral-antisemion theory  $\{1, \bar{s}\}$  instead. The corresponding channels can be constructed by just taking the Kraus operators to be the semion string operators. For the explicit expression of the shortest string operators of twisted  $\mathbb{Z}_2$  gauge theory, we refer the readers to the Supplemental Material of Ref. [110].

## V. DISCUSSION AND CONCLUSIONS

Our work introduces a promising mechanism for creating novel topologically ordered phases in mixed states. We give two complementary perspectives to demonstrate such a possibility. The first perspective is to look at what anyons are proliferated. One of our key observations is that while the routes of anyon condensation are limited for pure states, anyon proliferation in mixed states can occur in more general ways, offering new possibilities for topological order. In the three models studied in this work, we propose new types of topological order arising from incoherent proliferation of fermionic or semionic anyons in ground-state topological order, which drives an unconventional phase transition that does not resemble any anyon-condensation transition in pure states. The other perspective is to look at what remains. We find that the existence of anomalous strong 1-form symmetries can be viewed as a guiding principle for novel mixed-state TOs. We give general proof that anomalous strong 1-form symmetries imply the LRE nature of the mixed states, which manifests as deconfined anyons with nontrivial statistics. By analyzing the fusion rules and statistics of deconfined anyons, we show the possibility of realizing nonmodular TO in mixed states.

As is clear from the three examples, intrinsic mixed-state TOs can have or not have quantum memory, depending on whether the remaining deconfined anyons have nontrivial braiding statistics or only fermionic statistics [32].

It is worth noting that the construction of such exotic mixed states is experimentally feasible in current NISQ devices [17]. For example, one can realize the decohered  $\mathbb{Z}_2$  toric code model in Sec. II by implementing incomplete error correction, where only the error syndrome with  $A_v B_{p=v+\delta} = -1$  is corrected after the syndrome measurement using string operators  $W^e$  or  $W^m$ . This partial error correction would lead to a mixed state similar to  $\rho_f$ .

We end with some open directions. First, as already mentioned in Sec. III, it remains unclear whether 1-form symmetries generated by fermions also guarantee bipartite

long-range entanglement or whether there exist counterexamples that are bipartite separable but have multipartite long-range entanglement [66]. Second, a systematic classification of the intrinsic mixed-state TO is still lacking, with two main difficulties. The first is how to treat the weakly deconfined anyons with the peculiar one-way braiding statistics. The other is how to generalize the discussion of anyon statistics to mixed states away from the fixed-point models, such as the one discussed in Sec. IID. Finally, in our construction, we start from a topologically ordered state and obtain its descendants via noisy channels. It is also tempting to find systematic ways to prepare mixed-state topological order from short-range entangled mixed states by, e.g., measuring mixed-state symmetry-protected topological order [15,29,30,34,35].

### ACKNOWLEDGMENTS

We are especially grateful to Ruihua Fan for many pieces of valuable advice and feedback on the manuscript. We also thank Tsung-Cheng Lu for pointing out to us the dependence of the TEN on the choice of entanglement cut. We thank Yingfei Gu, Meng Cheng, Yu-An Chen, Zhen Bi, Jing-Yuan Chen, and He-Ran Wang for helpful discussions. This work is supported by the National Natural Science Foundation of China (NSFC) under Grant No. 12125405, the National Key R&D Program of China (Grant No. 2023YFA1406702), and the Innovation Program for Quantum Science and Technology (Grant No. 2021ZD0302502). Z. Wu acknowledges the support in part from Shuimu fellowships at Tsinghua University and the Engineering and Physical Sciences Research Council (EPSRC) fellowships.

## APPENDIX A: DETAILS ABOUT THE DECOHERED TORIC CODE

### 1. Calculation of the coherent information and mapping to the RBIM

In this appendix, we present detailed calculations of the coherent information  $I_c = S(\rho_f) - S(\rho_{Rf})$  and the derivation of the mapping to the RBIM along the Nishimori line [Eq. (4)] [71]. In the next two subsections, we calculate the two von Neumann entropies,  $S(\rho_f)$  and  $S(\rho_{Rf})$ , respectively, using the replica trick:  $S = -\text{Tr}(\rho \log \rho) = -\lim_{n \rightarrow 1} (\partial / \partial n) \text{Tr}(\rho^n)$ .

#### a. von Neumann entropy $S(\rho_{Rf})$

We begin with the calculation of  $S(\rho_{Rf})$ . We introduce two reference qubits, denoted by  $\sigma_{1,2}$ , and maximally entangle them with the two logical qubits in the ground-state subspace of the system

$$|\Psi\rangle = \frac{1}{2} \sum_{a,b=\pm 1} |a, b\rangle_S \otimes |\sigma_1^z = a, \sigma_2^z = b\rangle_R, \quad (\text{A1})$$

where  $a$  and  $b$  label the eigenvalues of the two noncontractible Wilson loops  $W_{\gamma_x}^z$  and  $W_{\gamma_y}^z$ , respectively, with the  $U(1)$  phase ambiguity fixed by

$$\begin{aligned} | -1, 1\rangle_S &= W_{\gamma_y}^x |1, 1\rangle_S, & |1, -1\rangle_S &= W_{\gamma_x}^x |1, 1\rangle_S, \\ | -1, -1\rangle_S &= W_{\gamma_y}^x W_{\gamma_x}^x |1, 1\rangle_S, \end{aligned} \quad (\text{A2})$$

where the  $W_{\gamma_{x,y}}^x$  are noncontractible  $X$  loops on the dual lattice. It is straightforward to check that  $|\Psi\rangle$  is a purification of  $\rho_0$ , the maximally mixed state in the ground-state subspace,  $\rho_0 = \text{tr}_R(|\Psi\rangle\langle\Psi|)$ . One can alternatively view the reference qubits as an input (via the Choi map), which encodes information into the code space [31].

To facilitate the calculation of the coherent information, we write the decohered  $\rho_{Rf}$  in the error-chain representation

$$\rho_{Rf} = \sum_C P(C) W_C^f |\Psi\rangle\langle\Psi| W_C^f, \quad (\text{A3})$$

where  $C$  denotes the error-chain configurations (the set of links where error occurs) with total length  $|C|$ .  $P(C) = p^{|C|}(1-p)^{N-|C|}$  is the occurrence probability of the error chain  $C$  [111].  $W_C^f$  is the (product of) open-string operators that create  $f$  anyons at the ends of the  $C$ .

Now, the trace  $\text{Tr}(\rho_{Rf}^n)$  is

$$\begin{aligned} \text{Tr}(\rho_{Rf}^n) &= \sum_{\{C^{(s)}\}} \prod_{s=1}^n P(C^{(s)}) \text{tr} \left[ \prod_{s=1}^n \left( W_{C^{(s)}}^f |\Psi\rangle\langle\Psi| W_{C^{(s)}}^f \right) \right], \\ &= \sum_{\{C^{(s)}\}} \prod_{s=1}^n P(C^{(s)}) \left\langle \Psi \left| W_{C^{(s)}}^f W_{C^{(s+1)}}^f \right| \Psi \right\rangle, \end{aligned} \quad (\text{A4})$$

where  $W_{C^{(n+1)}}^f \equiv W_{C^{(1)}}^f$  and the loops  $C^{(s)}$  satisfy

$$C^{(s+1)} = C^{(s)} + \partial v^{(s)}, \quad s = 1, 2, \dots, n-1 \quad (\text{A5})$$

to give a nonzero contribution. The  $\partial v^{(s)}$  are the boundaries of a set of plaquettes  $v^{(s)}$ , so they are homologically trivial loops. Then,  $\text{Tr}(\rho_{Rf}^n)$  can be further simplified as

$$\text{Tr}(\rho_{Rf}^n) = \frac{1}{2^{n-1}} \sum_{C^{(1)}} P(C^{(1)}) \sum_{\{v^{(s)}\}} \prod_{s=1}^{n-1} P(C^{(1)} + \partial v^{(s)}). \quad (\text{A6})$$

The prefactor  $1/2^{n-1}$  is due to the fact that for each replica  $s = 1, 2, \dots, n-1$ , there are two plaquette sets  $v^{(s)}$  giving the same boundary  $\partial v^{(s)}$ .  $\text{Tr}(\rho_{Rf}^n)$  can be mapped to the partition function of a classical Ising model with  $n-1$  flavors of Ising spin and a defect line at  $C^1$ . Concretely, we introduce  $Z_2$  variables  $n_{v^{(s)}}(l) = 1, 0$  to denote whether or

not link  $l$  is occupied in  $\partial v^{(s)}$ . We can then express the probability  $P(C^{(1)} + \partial v^{(s)})$  by the  $Z_2$  variables  $n_{v^{(s)}}(l)$ . For example, if a link  $l \in C^{(1)}$  and  $n_{v^{(s)}}(l) = 1$ , then link  $l$  does not occur in the error chain  $C^{(1)} + \partial v^{(s)}$  and contributes a factor  $(1-p)^{n_{v^{(s)}}(l)} p^{1-n_{v^{(s)}}(l)}$  in  $P(C^{(1)} + \partial v^{(s)})$ . As a result, the probability  $P(C^{(1)} + \partial v^{(s)})$  can be written as

$$P(C^{(1)} + \partial v^{(s)}) = \left[ \prod_{l \in C^{(1)}} \left( (1-p)^{n_{v^{(s)}}(l)} p^{1-n_{v^{(s)}}(l)} \right) \right] \times \left[ \prod_{l \notin C^{(1)}} \left( p^{n_{v^{(s)}}(l)} (1-p)^{1-n_{v^{(s)}}(l)} \right) \right]. \quad (\text{A7})$$

The first part with those links belonging to the error chain  $C^{(1)}$  can be made symmetric as

$$\begin{aligned} & \prod_{l \in C^{(1)}} \left( (1-p)^{n_{v^{(s)}}(l)} p^{1-n_{v^{(s)}}(l)} \right) \\ &= \prod_{l \in C^{(1)}} \left( \sqrt{p(1-p)} \left( \frac{1-p}{p} \right)^{n_{v^{(s)}}(l) - \frac{1}{2}} \right) \\ &= \sqrt{p(1-p)}^{|C^{(1)}|} \prod_{l \in C^{(1)}} \left( \frac{1-p}{p} \right)^{n_{v^{(s)}}(l) - \frac{1}{2}}. \quad (\text{A8}) \end{aligned}$$

Similarly, we also make the second part symmetric, as

$$\begin{aligned} & \prod_{l \notin C^{(1)}} \left( p^{n_{v^{(s)}}(l)} (1-p)^{1-n_{v^{(s)}}(l)} \right) \\ &= \prod_{l \notin C^{(1)}} \left( \sqrt{(1-p)p} \left( \frac{p}{1-p} \right)^{n_{v^{(s)}}(l) - \frac{1}{2}} \right) \\ &= \sqrt{p(1-p)}^{(N-|C^{(1)}|)} \prod_{l \notin C^{(1)}} \left( \frac{p}{1-p} \right)^{n_{v^{(s)}}(l) - \frac{1}{2}}. \quad (\text{A9}) \end{aligned}$$

Then, we can express the link-probability part  $(p/(1-p))^{n_{v^{(s)}}(l) - \frac{1}{2}}$  or  $((1-p)/p)^{n_{v^{(s)}}(l) - \frac{1}{2}}$  as an Ising coupling between two nearest-neighbor plaquettes that share the link  $l$ . Concretely, we introduce  $n-1$  flavors of Ising spins  $\tau^{(s)} = \pm 1, s = 1, 2, \dots, n-1$  on each plaquette and introduce the Ising coupling constant  $J$  as  $e^{-2J} = p/(1-p)$ . Then, the link-probability part  $(p/(1-p))^{n_{v^{(s)}}(l) - \frac{1}{2}}$  or  $((1-p)/p)^{n_{v^{(s)}}(l) - \frac{1}{2}}$  can be written as  $\exp[J\eta_{ij}\tau_i^{(s)}\tau_j^{(s)}]$ , where  $i$  and  $j$  are the dual lattice-site coordinates of the two plaquettes and  $\eta_{ij} = -1$  (1) for  $l$  belonging to (not belonging to) the error chain  $C^{(1)}$ . Then,  $p$  is the probability of antiferromagnetic coupling for each bond.

As a result,  $\text{Tr}(\rho_{Rf}^n)$  can be expressed as the partition function of an RBIM with  $n-1$  flavors of Ising spins and

periodic boundary condition (PBC)

$$\begin{aligned} \text{Tr}(\rho_{Rf}^n) &= \frac{1}{2^{n-1}} \sum_{C^{(1)}} P(C^{(1)}) \sum_{\{v^{(s)}\}} \prod_{s=1}^{n-1} P(C^{(1)} + \partial v^{(s)}) \\ &= \frac{1}{2^{n-1}} \left( \sqrt{(1-p)p} \right)^{(n-1)N} \sum_{C^{(1)}} P(\{\eta\}) \\ &\quad \times \sum_{\{\tau^{(s)}\}} \prod_{s=1}^{n-1} \exp \left[ J \eta_{ij} \tau_i^{(s)} \tau_j^{(s)} \right] \\ &= \frac{1}{2^{n-1}} \left( \sqrt{(1-p)p} \right)^{(n-1)N} \sum_{C^{(1)}} P(\{\eta\}) \\ &\quad \times \prod_{s=1}^{n-1} \sum_{\{\tau^s\}} \exp \left[ J \eta_{ij} \tau_i^{(s)} \tau_j^{(s)} \right] \\ &= \frac{1}{2^{n-1}} \left( \sqrt{(1-p)p} \right)^{(n-1)N} \sum_{C^{(1)}} P(\{\eta\}) (Z[J, \{\eta\}])^{n-1}. \quad (\text{A10}) \end{aligned}$$

Finally, we take the replica limit  $n \rightarrow 1$  to derive the von Neumann entropy  $S(\rho_{Rf})$ :

$$\begin{aligned} S(\rho_{Rf}) &= - \lim_{n \rightarrow 1} \frac{\partial}{\partial n} \text{Tr}(\rho_{Rf}^n) \\ &= - \frac{N}{2} \log[p(1-p)] + \log 2 \\ &\quad - \sum_{\{\eta\}} P(\{\eta\}) \log Z[J, \{\eta\}] \\ &\equiv - \overline{\log Z_{\text{PBC}}^{\text{RBIM}}} + \log 2 - \frac{N}{2} \log[p(1-p)], \quad (\text{A11}) \end{aligned}$$

where the first term is the average free energy of the RBIM along the Nishimori line:  $e^{-2J} = p/(1-p)$ .

## b. von Neumann entropy $S(\rho_f)$

The von Neumann entropy  $S(\rho_f)$  can be derived similarly to  $S(\rho_{Rf})$ . The initial density matrix is

$$\rho_0 = \frac{1}{4} \sum_{a,b=\pm 1} |a,b\rangle \langle a,b|. \quad (\text{A12})$$

Then,  $\text{Tr}(\rho_f^n)$  is

$$\begin{aligned} \text{Tr}(\rho_f^n) &= \sum_{\{C^{(s)}\}} \sum_{a^{(s)}, b^{(s)}} \prod_{s=1}^n P(C^{(s)}) \left( \frac{1}{4} \langle a^{(s)}, b^{(s)} | W_{C^{(s)}}^f W_{C^{(s+1)}}^f | a^{(s+1)}, b^{(s+1)} \rangle \right) \\ &= \frac{1}{2^{n-1}} \times \frac{1}{4^{n-1}} \sum_{C^{(1)}} P(C^{(1)}) \prod_{s=1}^{n-1} \sum_{\{v^{(s)}\}} \sum_{d_x^{(s)}, d_y^{(s)}=0,1} P(C^{(1)} + \partial v^{(s)} + d_x^{(s)} \gamma_x + d_y^{(s)} \gamma_y), \end{aligned} \quad (\text{A13})$$

where  $n+1 \equiv 1$  and  $d_{x,y}^{(s)} = 0, 1$  denotes whether or not  $C^{(s)}$  lies in the same homological class as  $C^{(1)}$ . Similarly to the mapping of  $\text{Tr}(\rho_{Rf}^n)$  to the partition function of RBIM, we can also map  $\text{Tr}(\rho_f^n)$  to the partition function of RBIM, except that here we must sum over the four contributions of inserting or not inserting the two noncontractible defect lines on the torus:

$$\begin{aligned} \text{Tr}(\rho_f^n) &= \frac{1}{2^{n-1}} \times \frac{1}{4^{n-1}} \left( \sqrt{(1-p)p} \right)^{(n-1)N} \sum_{C^{(1)}} P(\{\eta\}) \left( \sum_{d_x, d_y=0,1} Z_{d_x, d_y}[J, \{\eta\}] \right)^{n-1} \\ &\equiv \frac{1}{2^{n-1}} \times \frac{1}{4^{n-1}} \left( \sqrt{(1-p)p} \right)^{(n-1)N} \overline{\left( \sum_{d_x, d_y=0,1} Z_{d_x, d_y}^{\text{RBIM}} \right)^{n-1}}, \end{aligned} \quad (\text{A14})$$

where  $Z_{d_x, d_y}^{\text{RBIM}}$  is the partition function with  $d_a$  noncontractible defect lines inserted along the cycle  $\gamma_a$ . Along the defect line, the coupling changes from  $\eta J$  to  $-\eta J$ . This is equivalent to taking the antiperiodic boundary condition (APBC).

$S_{\rho_f}$  can in turn be obtained by taking the replica limit:

$$S(\rho_f) = - \lim_{n \rightarrow 1} \frac{\partial}{\partial n} \text{Tr}(\rho_f^n) = 3 \log 2 - \log \overline{\left[ \sum_{d_x, d_y=0,1} Z_{d_x, d_y}^{\text{RBIM}} \right]} - \frac{N}{2} \log[p(1-p)]. \quad (\text{A15})$$

We note that the second term can also be understood as the free energy of RBIM with all four types of boundary condition (PBC or APBC along the  $x$  or  $y$  direction) into account.

### c. Critical error rate and classical memory from coherent information

As we have demonstrated in the previous subsections,  $S_{\rho_f}$  and  $S_{\rho_{Rf}}$  can be mapped to the free energy of the RBIM with or without the insertion of noncontractible defect lines (plus some constants), so the coherent information  $I_c$  is related to the excess free energy of the defect line,

$$I_c = 2 \log 2 - \log \frac{\overline{\sum_{d_x, d_y=0,1} Z_{d_x, d_y}^{\text{RBIM}}}}{Z_{00}^{\text{RBIM}}} = 2 \log 2 - \log \overline{\left[ \sum_{d_x, d_y=0,1} e^{-\Delta F_{d_x, d_y}} \right]}, \quad (\text{A16})$$

where  $\Delta F_{d_x, d_y}$  is the excess free energy with the insertion of a noncontractible defect line. For small  $p$ , the RBIM is in the ferromagnetic (FM) phase and the excess free energy of a defect line is extensive,  $\Delta F_{\{d_x, d_y\} \neq (0,0)} \sim O(L)$ , which leads to  $I_c = 2 \log 2$ . On the other hand, when  $p$  is above the error threshold  $p_c \approx 0.109$ , the RBIM undergoes a phase transition to a paramagnetic (PM) phase and  $I_c$  drops to 0 in the thermodynamic limit, which indicates that  $\rho_f$  only retains a classical memory. This

is exactly the same as the situation with single-qubit errors.

## 2. Relative entropy

As mentioned in the main text, the phase transition at  $p_f = p_c$  is driven by the proliferation of  $f$  anyons. In the double space, this corresponds to the condensation of  $f_+ f_-$ . In this section, we provide a quantitative

diagnosis of the  $f$  anyon proliferation in the original Hilbert space. We denote the string operators creating  $\alpha$  anyons at the ends of the string as  $w^\alpha$ , and investigate whether  $\rho_f^\alpha \equiv \mathcal{N}^f [w^\alpha \rho_0 w^\alpha]$  is really a distinct state from  $\rho_f$ . Quantitatively, we calculate the relative entropy,

$$D(\rho_f || \rho_f^\alpha) \equiv \text{Tr}(\rho_f \log \rho_f) - \text{Tr}(\rho_f \log \rho_f^\alpha), \quad (\text{A17})$$

and examine whether it diverges as the length of  $w^\alpha$  approaches infinity, which is proposed as a generalization of the Fredenhagen-Marcu order parameter for ground states [31,112,113].

Using the error-chain expansion, we obtain

$$\begin{aligned} \text{Tr} \rho_f (\rho_f^\alpha)^{n-1} &= \sum_{\{C^{(s)}\}} \prod_{s=1}^n P(C^{(s)}) \text{Tr} \left( W_{C^{(1)}}^f \rho_0 W_{C^{(1)}}^f \prod_{s=2}^n W_{C^{(s)}}^f w^\alpha \rho_0 w^\alpha W_{C^{(s)}}^f \right) \\ &= \sum_{\{C^{(s)}\}} \sum_{\{a^{(s)}, b^{(s)}\}} \left[ \prod_{s=1}^n \frac{1}{4} P(C^{(s)}) \right] \langle a^{(1)}, b^{(1)} | W_{C^{(1)}}^f W_{C^{(2)}}^f w^\alpha | a^{(2)}, b^{(2)} \rangle \langle a^{(n)}, b^{(n)} | w^\alpha W_{C^{(n)}}^f W_{C^{(1)}}^f | a^{(1)}, b^{(1)} \rangle \\ &\quad \prod_{s=2}^{n-1} \langle a^{(s)}, b^{(s)} | w^\alpha W_{C^{(s)}}^f W_{C^{(s+1)}}^f w^\alpha | a^{(s+1)}, b^{(s+1)} \rangle. \end{aligned} \quad (\text{A19})$$

Clearly, for  $\alpha = e, m$ ,  $\text{Tr} \rho_f (\rho_f^\alpha)^{n-1} = 0$ , so the relative entropy diverges. Thus, in what follows, we only focus on  $\alpha = f$ . Terms in the summation are nonvanishing only if the error-chain configurations satisfy the following condition:

$$\begin{aligned} C^{(s)} &= C^{(1)} + \partial v^{(s)} + d_x^{(s)} \gamma_x + d_y^{(s)} \gamma_y + A, \\ s &= 1, 2, \dots, n-1, \end{aligned} \quad (\text{A20})$$

where  $d_{x/y}^{(s)} = 0, 1$  and  $A$  denotes the string where  $w^{\alpha=f}$  acts nontrivially. Compared to Eqs. (A13) and (A14), we can see that the insertion of  $w_A^f$  corresponds to inserting an additional defect line along  $A$  in the RBIM, which means that the Ising coupling flips sign along  $A$ . We denote the partition function of RBIM with a defect line along  $A$  as  $Z^{\text{RBIM}}[A]$ , where we implicitly sum over the four types of boundary conditions  $\{d_x, d_y\}$ . Then,

$$D^{(n)}(\rho_f || \rho_f^f) = \frac{1}{1-n} \log \frac{(Z^{\text{RBIM}}[A])^{n-1}}{(Z^{\text{RBIM}})^{n-1}}. \quad (\text{A21})$$

Taking the replica limit  $n \rightarrow 1$ , we obtain the relative entropy,

$$D(\rho_f || \rho_f^f) = \overline{\log Z^{\text{RBIM}}} - \overline{\log Z^{\text{RBIM}}[A]}, \quad (\text{A22})$$

It turns out that, for  $p_f < p_c$ ,  $D(\rho_f || \rho_f^\alpha)$  diverges for all three types of anyons, while for  $p_f > p_c$ ,  $D(\rho_f || \rho_f^f)$  becomes finite, in agreement with our expectation. Additionally, although  $D(\rho_f || \rho_f^{e(m)})$  is divergent,  $e$  and  $m$  cease to be distinct (weakly) deconfined excitations, since  $e \times f = m$ .

To obtain  $D(\rho_f || \rho_f^\alpha)$ , we can still use the replica trick:

$$D^{(n)}(\rho_f || \rho_f^\alpha) \equiv \frac{1}{1-n} \log \frac{\text{Tr} \rho_f (\rho_f^\alpha)^{n-1}}{\text{Tr} \rho_f^n} \quad (\text{A18})$$

and recover  $D(\rho_f || \rho_f^\alpha)$  by taking the limit  $n \rightarrow 1$ .

which is mapped to the excess free energy of defect line  $A$ . In the FM phase ( $p < p_c$ ), it diverges as the distance between the two ends of  $A$  goes to infinity. However, in the PM phase ( $p > p_c$ ), it is finite, which indicates the incoherent proliferation of  $f$ .

### 3. Calculation of the entanglement negativity

In this section, we derive the entanglement negativity  $\varepsilon_A(\rho_f) \equiv \log ||\rho_f^{T_A}||_1$ . It turns out that to calculate  $\varepsilon_A(\rho_f)$ , it is more convenient to use the loop expansion [Eq. (7)] instead of the error-chain expansion used in the last two sections. We start from Eq. (9):

$$\rho_f^{T_A} = \frac{1}{2^N} \sum_{g \in G} (1-2p)^{l_g} y_A(g) g, \quad (\text{A23})$$

where  $l_g$  is the length of the segment where  $g_x$  and  $g_z$  do not coincide and

$$y_A(g) \equiv \text{sign}_A(g_x, g_z) \equiv \begin{cases} 1, & \text{if } g_{xA}, g_{zA} \text{ commute,} \\ -1, & \text{if } g_{xA}, g_{zA} \text{ anticommute.} \end{cases}$$

To calculate  $\varepsilon_A(\rho_f)$ , we utilize the replica trick, i.e., we first calculate the  $2n$ th Renyi negativity  $\varepsilon_A^{(2n)}(\rho_f) :=$



$(1/(2-2n)) \log(\text{Tr}(\rho_f^{T_A})^{2n}/\text{Tr}(\rho_f)^{2n})$  and finally take the replica limit  $2n \rightarrow 1$ .

First, we consider the bipartition of  $A \cup \bar{A}$  of a cylinder, as shown in Figs. 1(g)–1(i). We denote the bipartition in Fig. 1(h) as bipartition 1 and that in Fig. 1(i) as bipartition 2. We discuss these two types of bipartitions in detail below.

*Bipartition 1, generic  $p$ .* We deal with bipartition 1 first. In this case, we are able to obtain an exact result of  $\varepsilon_A^{(2n)}$  for any  $p$ . As we will show below, the result actually does not depend on  $p$  at all. To start with, we calculate  $(\rho_f^{T_A})^2$ :

$$\begin{aligned} (\rho_f^{T_A})^2 &= \frac{1}{2^{2N}} \sum_{g,h \in G} (1-2p)^{l_g+l_h} y_A(g) y_A(h) gh \\ &= \frac{1}{2^{2N}} \sum_{g,h \in G} (1-2p)^{l_g+l_h} y_A(gh) \text{sign}_A(g,h) gh \\ &= \frac{1}{2^{2N}} \sum_{g,\tilde{g} \in G} (1-2p)^{l_g+l_{\tilde{g}}} y_A(\tilde{g}) \text{sign}_A(g,\tilde{g}) \tilde{g}. \end{aligned} \quad (\text{A24})$$

In the last step, we use the substitution  $h = g\tilde{g}$ .

To simplify the expression, we deal with the summation over  $g$  first. The crucial part in this expression is  $\text{sign}_A(g,\tilde{g})$ , which leads to complete destructive interference when  $\tilde{g}$  crosses the boundary between  $A$  and  $\bar{A}$ . To be more precise, we define the subgroup  $H$  of  $G$ :

$$H \equiv \{g \in G \mid g_A g'_A = g'_A g_A, \forall g' \in G\}. \quad (\text{A25})$$

For bipartition 1,  $H$  contains all loops that do not cross the boundary. Then, we can simplify Eq. (A24):

$$(\rho_f^{T_A})^2 = \frac{1}{2^{2N}} \sum_{g \in G, \tilde{g} \in H} (1-2p)^{l_g+l_{\tilde{g}}} y_A(\tilde{g}) \tilde{g}. \quad (\text{A26})$$

Thus,

$$\begin{aligned} \text{Tr}(\rho_f^{T_A})^{2n} &= 2^{-2nN} \prod_{s=1}^n \sum_{\tilde{g}^{(s)} \in H} \prod_{s=1}^n \sum_{g^{(s)} \in G} (1-2p)^{\sum_{s=1}^n l_{g^{(s)}} + l_{g^{(s)}\tilde{g}^{(s)}}} y_A(\prod_{s=1}^n \tilde{g}^{(s)}) \text{Tr} \left( \prod_{s=1}^n \tilde{g}^{(s)} \right) \\ &= 2^{(1-2n)N} \sum_{\tilde{g}^{(1)}, \dots, \tilde{g}^{(n-1)} \in H} \sum_{g^{(1)}, \dots, g^{(n)} \in G} (1-2p)^{\sum_{s=1}^{n-1} (l_{g^{(s)}} + l_{g^{(s)}\tilde{g}^{(s)}}) + l_{\prod_{s=1}^{n-1} g^{(s)}} + l_{\prod_{s=1}^{n-1} g^{(s)}\tilde{g}^{(s)}}}. \end{aligned} \quad (\text{A27})$$

In a similar manner we can obtain  $\text{Tr} \rho_f^{2n}$ , resulting in a similar expression with the summation over  $H$  replaced by a summation over  $G$ :

$$\text{Tr} \rho_f^{2n} = 2^{(1-2n)N} \sum_{\tilde{g}^{(1)}, \dots, \tilde{g}^{(n-1)} \in G} \sum_{g^{(1)}, \dots, g^{(n)} \in G} (1-2p)^{\sum_{s=1}^{n-1} (l_{g^{(s)}} + l_{g^{(s)}\tilde{g}^{(s)}}) + l_{\prod_{s=1}^{n-1} g^{(s)}} + l_{\prod_{s=1}^{n-1} g^{(s)}\tilde{g}^{(s)}}}. \quad (\text{A28})$$

Since we are only concerned about their ratio, we can extract the common part in the expression and rename it as  $O_{\{\tilde{g}\}}$ :

$$O_{\{\tilde{g}\}} = 2^{(1-2n)N} \sum_{g^{(1)}, \dots, g^{(n)} \in G} (1-2p)^{\sum_{s=1}^{n-1} (l_{g^{(s)}} + l_{g^{(s)}\tilde{g}^{(s)}}) + l_{\prod_{s=1}^{n-1} g^{(s)}} + l_{\prod_{s=1}^{n-1} g^{(s)}\tilde{g}^{(s)}}}. \quad (\text{A29})$$

It is straightforward to show that  $O_{\{\tilde{g}\}}$  is actually only a function of  $l_{\tilde{g}^{(s)}}$ . Based on this observation, we can divide the summation over  $\{\tilde{g}\}$  into different classes. First, we define the invariant subgroup  $G_f$  of  $G$ , generated by  $A_{v=p-\delta} B_p$ . In other words, elements in  $G_f$  are tensionless loops with  $l_g = 0$ . Similarly, we define the subgroup  $H_f$  of  $H$  to be  $H_f \equiv \{g \in G_f \mid g_A g'_A = g'_A g_A, \forall g' \in G_f\}$ . Then,

$$\begin{aligned}\mathrm{Tr}(\rho_f^{T_A})^{2n} &= \sum_{\tilde{g}_f^{(1)}, \dots, \tilde{g}_f^{(n-1)} \in H_f} \sum_{\tilde{u}^{(1)}, \dots, \tilde{u}^{(n-1)} \in H/H_f} O_{\{\tilde{u}\}}, \\ \mathrm{Tr}\rho_f^{2n} &= \sum_{\tilde{g}_f^{(1)}, \dots, \tilde{g}_f^{(n-1)} \in G_f} \sum_{\tilde{u}^{(1)}, \dots, \tilde{u}^{(n-1)} \in G/G_f} O_{\{\tilde{u}\}}\end{aligned}\quad (\text{A30})$$

Since  $G/G_f = H/H_f$ , we obtain

$$\frac{\mathrm{Tr}(\rho_f^{T_A})^{2n}}{\mathrm{Tr}\rho_f^{2n}} = \left(\frac{|H_f|}{|G_f|}\right)^{n-1} = 2^{(2-2n)(L-1)}, \quad (\text{A31})$$

where  $L$  is the length of the entanglement cut. Thus the Renyi negativity is

$$\varepsilon_A^{(2n)}(\rho_f) = (L-1) \log 2, \forall n. \quad (\text{A32})$$

In the replica limit  $2n \rightarrow 1$ , we obtain  $\varepsilon_A(\rho_f) = (L-1) \log 2$ . The subleading term,  $\log 2$ , is the TEN, which takes exactly the same value as that of the toric code ground state.

*Bipartition 2*,  $p = \frac{1}{2}$ . For bipartition 2, the calculation for generic  $p$  is much more challenging. This is mainly because  $G/G_f \neq H/H_f$ , which means that Eq. (A31) cannot be derived from Eq. (A30) for generic  $p$ . As a result, the negativity does depend on  $p$  for this bipartition. Here, we are mainly interested in the phase with intrinsic mixed-state TOs for  $p > p_c$ , so we take the maximally decohered limit,  $p = \frac{1}{2}$ , in which case the calculation can be greatly simplified.

For  $p = \frac{1}{2}$ ,

$$\rho_f = \frac{1}{2^N} \sum_{g_f \in G_f} g_f = \frac{1}{2^{N/2+1}} \prod_p \frac{1+W_p}{2}, \quad W_p := A_{p-\delta} B_p. \quad (\text{A33})$$

In this case, the negativity exhibits an unusual dependence on the parity of  $L$ , as shown in Eq. (12). We will derive this result below.

Analogously to Eqs. (A24) and (A26), we have

$$\begin{aligned}(\rho_f^{T_A})^2 &= \frac{1}{2^{2N}} \sum_{g_f, \tilde{g}_f \in G_f} y_A(\tilde{g}_f) \mathrm{sign}_A(g_f, \tilde{g}_f) \tilde{g}_f \\ &= \frac{1}{2^{2N}} \sum_{g_f \in G_f, \tilde{g}_f \in H_f} y_A(\tilde{g}_f) \tilde{g}_f.\end{aligned}\quad (\text{A34})$$

Then, it is straightforward to obtain the Renyi negativity:

$$\varepsilon_A^{(2n)}(\rho_f) = \frac{1}{2-2n} \log \left( \frac{|H_f|}{|G_f|} \right)^{n-1}. \quad (\text{A35})$$

For odd  $L$ ,  $|G_f|/|H_f|$  amounts to the number of elements in  $G_f$  acting on the boundary:  $|G_f|/|H_f| =$

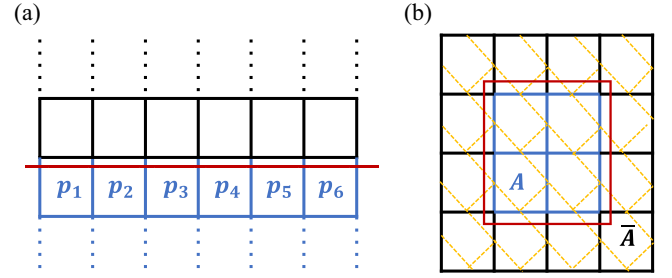


FIG. 9. (a) Bipartition 2 on a cylinder; in this case,  $L = 6$ . (b) An example of bipartition with contractible subregion  $A$ . The orange dashed lines represent auxiliary links. In this case,  $N_f = 12$ .

$2^{L-1}$ . Here, the “ $-1$ ” is due to the fact that  $h = \prod_{p_i \text{ on the boundary}} W_{p_i}$  is an element in  $H_f$ . Consequently,  $\varepsilon_A^{(2n)}(\rho_f) = ((L-1)/2) \log 2$ . The negativity is half the value for bipartition 1, because there are only half as many  $W_p$  acting on the boundary.

For even  $L$ , the calculation is more subtle. Specifically, there exist special elements  $h_1 = \prod_{i=1,3,\dots,L-1} W_{p_i}$ ,  $h_2 = \prod_{i=2,4,\dots,L} W_{p_i} (= h \times h_1)$ , that act nontrivially on the boundary, but still belong to  $H_f$  [for an illustration, see Fig. 9(a)]. Therefore,  $|G_f|/|H_f| = 2^{L-2}$ ,  $\varepsilon_A^{(2n)}(\rho_f) = ((L-2)/2) \log 2$ .

Taking the replica limit  $2n \rightarrow 1$ , we obtain the final result of the logarithmic negativity (for bipartition 2):

$$\varepsilon_A(\rho_f) = \begin{cases} \frac{L}{2} \log 2 - \log 2, & \text{if } L \text{ is even,} \\ \frac{L}{2} \log 2 - \frac{\log 2}{2}, & \text{if } L \text{ is odd.} \end{cases} \quad (\text{A36})$$

In all the cases, we obtain a nonzero TEN, indicating nontrivial topological order. Here, the value of the TEN exhibits an unusual dependence on the parity of the boundary size and thus seems to be less universal than we would expect for a topologically ordered phase. In Appendix A 4, we will try to resolve this puzzle by relating the entanglement properties of  $\rho_f$  to those of more familiar ground-state topological order.

Before that, we first make some quick comments on entanglement negativity for more generic bipartitions, including the cases with contractible subregion  $A$ . For  $p = \frac{1}{2}$ , we can perform calculations similar to those shown above and get exact results of negativity with general bipartitions. It is convenient to introduce some auxiliary links connecting the six qubits acted upon by  $W_p$  for each  $p$ . We give one example in Fig. 9(b). With the help of these auxiliary links, the entanglement negativity for general bipartitions (with the only assumption being that both

$A$  and  $\bar{A}$  are connected) yields

$$\varepsilon_A(\rho_f) = \begin{cases} \frac{N_l}{2} \log 2 - \log 2, & \text{if } N_l \text{ is even,} \\ \frac{N_l}{2} \log 2 - \frac{\log 2}{2}, & \text{if } N_l \text{ is odd.} \end{cases} \quad (\text{A37})$$

$N_l$  counts the number of auxiliary links that are cut through by the entanglement cut. The even or odd dependence shows up again. The reason that bipartition 1 is free of this problem is that  $N_l = 2L$  is always even in that case. Finally, we note that due to the unusual dependence of the TEN (defined as the value of the subleading term here) on the boundary size, one cannot extract the TEN by calculating the tripartite mutual information as in the Kitaev-Preskill scheme, unless one carefully chooses the multipartition such that the  $N_l$  have the same parity for all subregions.

#### 4. Relation to translation-symmetry-enriched $\mathbb{Z}_2$ TO

In this section, we give an explanation of the curious dependence of the TEN on the entanglement cut, by establishing a connection between the entanglement properties of  $\rho_f$  and ground-state  $Z_2$  topological order enriched by translation symmetry. To establish this connection, we first note that at  $p = \frac{1}{2}$ ,  $\rho_f$  is nothing but the maximally mixed state with  $W_p = A_{p-\delta} B_p = 1, \forall p$ . To find its analog in ground states of local Hamiltonians, it is natural design a stabilizer code with  $W_p$  being the stabilizers. Of course, without other terms, we would get a very large ground-state degeneracy, and the maximally mixed states in the ground-state subspace would just be  $\rho_f$ . Thus we need more stabilizers. Here, we provide one illuminating choice:

$$H_{\text{SET}} = - \sum_p W_p - \sum_{\text{vertical link } i} Z_i X_{i+\delta}. \quad (\text{A38})$$

It is straightforward to check that all the terms in  $H_{\text{SET}}$  commute with each other and that the ground state is determined up to topological degeneracy. Actually, this model has recently been constructed and studied in Ref. [114]. We briefly summarize the important properties of this model:

- (1) It has  $Z_2$  (toric code) topological order, i.e., it has the same type of anyon excitations and the same statistics as the toric code.
- (2) In this model, the  $Z_2$  topological order is enriched by translation symmetry along the horizontal direction, which is manifested in the fact that excitations  $W_p = -1$  for  $p$  on even columns and odd columns belong to different anyon superselection sectors and correspond to  $e$  and  $m$  anyons in the toric code, respectively. This phenomenon is often called weak symmetry breaking.
- (3) As a consequence of weak symmetry breaking, the ground-state degeneracy (GSD) on a torus depends

on the linear size along the horizontal direction, denoted by  $L_x$ : GSD = 4(2) for even (odd)  $L_x$ .

Our primary goal for introducing this model is to understand the weird behavior of the entanglement negativity for bipartition 2 given in Eq. (A37)  $\rho_f$  for bipartition 2, so we consider putting the model of Eq. (A38) on a cylinder and investigate the entanglement property of the ground state under the same bipartition. First, we note that the ground state or, more specifically, the maximally mixed state in the ground-state subspace, can be written in an illuminating way:  $\rho_{\text{GS}} \propto \rho_f \prod_{\text{vertical link } i} ((1 + Z_i X_{i+\delta})/2)$ . Moreover, for bipartition 2, the entanglement cut does not go through the stabilizers  $Z_i X_{i+\delta}$  at all, so these stabilizers contribute zero entanglement. Thus,

$$\varepsilon_A(\rho_{\text{GS}}) = \varepsilon_A(\rho_f) = \begin{cases} \frac{L_x}{2} \log 2 - \log 2, & \text{if } L_x \text{ is even,} \\ \frac{L_x}{2} \log 2 - \frac{\log 2}{2}, & \text{if } L_x \text{ is odd.} \end{cases} \quad (\text{A39})$$

We can instead calculate the entanglement entropy  $S_A$  for a (pure) ground state, with a bit more complication. To do this, we first need to specify the boundary conditions at the upper and lower boundaries of the cylinder (nevertheless, the result does not depend on the choice of the boundary conditions). Then, by fixing the value of the logical string operators along the horizontal direction, we can obtain a pure state and calculate its bipartite entanglement entropy, which yields the same result:

$$S_A = \begin{cases} \frac{L_x}{2} \log 2 - \log 2, & \text{if } L_x \text{ is even,} \\ \frac{L_x}{2} \log 2 - \frac{\log 2}{2}, & \text{if } L_x \text{ is odd.} \end{cases} \quad (\text{A40})$$

Thus, the TEN of  $\rho_f$  can be directly related to the TEE or TEN of the ground state of  $H_{\text{SET}}$ . For the latter, the dependence of the TEE or TEN on the parity of  $L_x$  is a common feature of topological order with weak symmetry breaking of translations and can be understood in the following way. Since translations permute  $e$  and  $m$ , for odd  $L_x$ ,  $e$  and  $m$  are exchanged when going around the cylinder (along the  $x$  direction) once. Thus, instead of two independent logical string operators along the  $x$  direction as naively expected (for even  $L_x$ , the two logical string operators can be constructed by creating a pair of  $e$  or  $m$  anyons, dragging one of them around a cycle, and annihilating the pair), only one can be found. This subtlety here causes the TEE or TEN as well as the GSD to have only half the value expected for the toric code topological order.

### 5. Robustness under phase errors

In this section, we aim to discuss the robustness of the intrinsic mixed-state topological order under other noises. We demonstrate how to obtain the phase diagram in Fig. 2 with additional single-qubit phase errors. Concretely, we consider the following mixed state:

$$\rho_{f,e} = \mathcal{N}^z \circ \mathcal{N}^f [\rho_0]. \quad (\text{A41})$$

Similar to Appendixes A 1 and A 2, we analyze the properties of  $\tilde{\rho}_f$  by calculating the von Neumann entropy  $S(\tilde{\rho}_f)$  and mapping it to a statistical model.

We denote the error rate and error-chain configuration of  $\mathcal{N}^z$  ( $\mathcal{N}^f$ ) as  $p_z$  ( $p_f$ ) and  $C_z$  ( $C_f$ ), respectively. Then  $\rho_{f,e}$  can be represented by the error-chain expansion as in Eq. (A3):

$$\rho_{f,e} = \sum_{C_z, C_f} P_f(C_f) P_z(C_z) W_{C_f}^f W_{C_z}^e \rho_0 W_{C_z}^e W_{C_f}^f. \quad (\text{A42})$$

Then, we can write the  $n$ th moment as

$$\text{Tr}(\rho_{f,e}^n) = \sum_{\{C^{(s)}\}} \sum_{a^{(s)}, b^{(s)}} \prod_{s=1}^n \frac{1}{4} P_f(C_f^{(s)}) P_z(C_z^{(s)}) \langle a^{(s)}, b^{(s)} | W_{C_z^{(s)}}^e W_{C_f^{(s)}}^f W_{C_f^{(s+1)}}^f W_{C_z^{(s+1)}}^e | a^{(s+1)}, b^{(s+1)} \rangle. \quad (\text{A43})$$

Nonzero contributions only come from error-chain configurations satisfying

$$C_z^{(s)} = C_z^{(1)} + \partial v^{(s)} + d_x^{z,(s)} \gamma_x + d_x^{z,(s)} \gamma_y, \quad C_f^{(s)} = C_f^{(1)} + \partial v^{(s)} + d_x^{f,(s)} \gamma_x + d_x^{f,(s)} \gamma_y, \quad (\text{A44})$$

so Eq. (A43) can be simplified as

$$\text{Tr}(\rho_{f,e}^n) = \frac{1}{4^{n-1}} \times \frac{1}{4^{n-1}} \prod_{\alpha=z,f} \left[ \sum_{C_\alpha^{(s)}} P(C_\alpha^{(1)}) \prod_{s=1}^{n-1} \sum_{\{v_\alpha^{(s)}\}} \sum_{d_x^{\alpha,(s)}, d_y^{\alpha,(s)}=0,1} P(C_\alpha^{(1)} + \partial v_\alpha^{(s)} + d_x^{\alpha,(s)} \gamma_x + d_y^{\alpha,(s)} \gamma_y) \right]. \quad (\text{A45})$$

As in Eq. (A14), the collection of terms in the bracket for each  $\alpha$  can be mapped to the partition function of a  $(n-1)$ -flavor RBIM:

$$\text{Tr}(\rho_{f,e}^n) = \frac{1}{4^{2n-2}} \left( \sqrt{(1-p_f)p_f} \right)^{(n-1)N} \left( \sqrt{(1-p_z)p_z} \right)^{(n-1)N} \overline{\left( Z_{p_f}^{\text{RBIM}}(J_f) \right)^{n-1}} \times \overline{\left( Z_{p_z}^{\text{RBIM}}(J_z) \right)^{n-1}}, \quad (\text{A46})$$

where  $J_\alpha$  ( $\alpha = z, f$ ) is the strength of the Ising coupling for each of the two RBIMs.  $p_\alpha$  denotes the probability of antiferromagnetic coupling on each bond. Both RBIMs are situated along the Nishimori line:  $e^{-2J_\alpha} = p_\alpha / (1 - p_\alpha)$ . Again, the partition functions implicitly contain summations over the four boundary conditions. The von Neumann entropy can be obtained by taking the limit as  $n \rightarrow 1$ :

$$\begin{aligned} S(\rho_{f,e}) &= - \lim_{n \rightarrow 1} \frac{\partial}{\partial n} \text{Tr}(\rho_{f,e}^n) \\ &= - \overline{\log Z_{p_z}^{\text{RBIM}}(J_z)} - \overline{\log Z_{p_f}^{\text{RBIM}}(J_f)} + \left( -4 \log 2 - \frac{N}{2} \log[p_z(1-p_z)] - \frac{N}{2} \log[p_f(1-p_f)] \right). \end{aligned} \quad (\text{A47})$$

The terms in the parentheses are always regular for finite  $p_z, p_f$ , so we can focus on the first two terms, which are the free energies of two decoupled RBIMs. We denote the Ising spin variables of the two RBIMs as  $\sigma$  and  $\tau$ ,

respectively. Then we can straightforwardly obtain the phase diagram of the statistical model, shown in Fig. 2.

Applying the same strategy as in Appendixes A 1 and A 2, we can map the relative entropy and coherent

information to observables in the RBIM. We directly list the results here:

- (1) Relative entropy:  $D(\rho_{f,e} || \rho_{f,e}^e)$  is mapped to the excess free energy of the defect line (connecting the inserted pair of  $e$  anyons) of the RBIM of spin  $\sigma$ ;  $D(\rho_{f,e} || \rho_{f,e}^f)$  is mapped to the excess free energy of the defect line (connecting the inserted pair of  $f$  anyons) of the RBIM of spin  $\tau$ ;  $D(\rho_{f,e} || \rho_{f,e}^m)$  is mapped to the sum of the excess free energy of the defect line (connecting the inserted pair of  $m$  anyons) of the two RBIMs, because  $w^m = w^e w^f$ .
- (2) Coherent information:

$$I_c = 2 \log 2 - \log \left[ \sum_{d_x, d_y=0,1} e^{-\Delta F_{d_x, d_y}^\sigma} \right] - \log \left[ \sum_{d_x, d_y=0,1} e^{-\Delta F_{d_x, d_y}^\tau} \right], \quad (\text{A48})$$

where  $\Delta F_{d_x, d_y}^{\sigma(\tau)}$  is the excess free energy of noncontractible defect lines in the RBIM of spin  $\sigma$  ( $\tau$ ). Across transitions at  $p_z \approx 0.109$  and  $p_f \approx 0.109$ ,  $I_c$  changes discontinuously. Quantum memory can only be realized when both  $\sigma$  and  $\tau$  are in the FM phase, while classical memory corresponds to one of the spin species being in the FM phase while the other in the PM phase and the topological memory is completely lost when both RBIMs are in the PM phase.

From the above mapping, we can relate the four phases of the RBIM to the four types of topological order (including the trivial one) in Fig. 2.

## APPENDIX B: EXACT SOLUTION TO THE GAPLESS SPIN LIQUID PHASE OF THE TORIC CODE MODEL THROUGH FERMIONIZATION

In this appendix, we analyze the properties of the toric code model with additional  $ZX$  terms in the Hamiltonian,

$$H = - \sum_v A_v - \sum_p B_p - \sum_i h_{xz} Z_i X_{i+\delta}. \quad (\text{B1})$$

We show that this model can be solved exactly using the method introduced in Ref. [85]. First, we note that the model has an extensive number of locally conserved quantities.  $[H, W_p] = 0$  with  $W_p = A_{v=p-\delta} B_p$ , which follows from the fact that the  $e$  anyons and adjacent  $m$  anyons are always created or annihilated in pairs, so we can solve the model in each simultaneous eigenspace of  $W_p$ . Second, the role of the  $ZX$  term is to induce pair creation, annihilation, and hopping of  $f$  anyons, which are fermions. Then, on an infinite lattice or a topologically trivial lattice, in each sector  $\{W_p = w_p\}$ , the only degrees of freedom are the  $f$  anyons, so we expect that in each sector, the model can be described by a fermion tight-binding model. We assume that the fermions are defined on the vertices of the lattice, with the mapping

$$n_v^f \longleftrightarrow \frac{1 - A_v}{2}, \quad (\text{B2})$$

where  $n_v^f = f_v^\dagger f_v$  is the fermion-number operator. This mapping follows naturally from the observation that in the zero-flux sector  $\{w_p = 1\}$ ,  $(1 - A_v)/2$  corresponds to the occupation number of the  $f$  anyon on  $v$ . Finally, because  $f$  and  $e/m$  anyons are mutual semions, an  $f$  anyon can acquire a nontrivial phase depending on  $w_p$  when moving around the plaquette  $p$ . Thus  $W_p$  should correspond to static  $Z_2$  flux on each plaquette in the fermion model and so we have the following mapping:

$$T_{v_i v_i'} \equiv i u_i \gamma_{v_i} \gamma_{v_i'}' \longleftrightarrow Z_i X_{i+\delta}, \quad \text{link } i \equiv \langle v_i v_i' \rangle \quad (\text{B3})$$

where the  $\gamma_v = f_v + f_v^\dagger$ ,  $\gamma_{v'}' = -i(f_{v'} - f_{v'}^\dagger)$  are Majorana-fermion operators and the  $u_i = \pm 1$  are static  $Z_2$  gauge fields defined on links, as depicted in Fig. 10. It is straightforward to check that the commutation and anticommutation relation between  $Z_i X_{i+\delta}$  is preserved under the above mapping:

$$\left\{ \begin{array}{l} \{T_{v_i v_i'}, T_{v_j v_j'}\} = 0, \quad \text{if } i = j \pm \delta, \\ [T_{v_i v_i'}, T_{v_j v_j'}] = 0, \quad \text{otherwise,} \end{array} \right\} \longleftrightarrow \left\{ \begin{array}{l} \{Z_i X_{i+\delta}, Z_j X_{j+\delta}\} = 0, \quad \text{if } i = j \pm \delta, \\ [Z_i X_{i+\delta}, Z_j X_{j+\delta}] = 0, \quad \text{otherwise.} \end{array} \right. \quad (\text{B4})$$

The commutation and anticommutation relation between  $Z_i X_{i+\delta}$  and  $A_v$  (and similarly for  $B_p = A_{v=p-\delta} W_p$ ) is also preserved:

$$\left\{ \begin{array}{l} \{T_{v_i v_i'}, 1 - 2n_v^f\} = 0, \quad \text{if } v \in \partial i, \\ [T_{v_i v_i'}, 1 - 2n_v^f] = 0, \quad \text{otherwise,} \end{array} \right\} \longleftrightarrow \left\{ \begin{array}{l} \{Z_i X_{i+\delta}, A_v\} = 0, \quad \text{if } v \in \partial i, \\ [Z_i X_{i+\delta}, A_v] = 0, \quad \text{otherwise.} \end{array} \right. \quad (\text{B5})$$

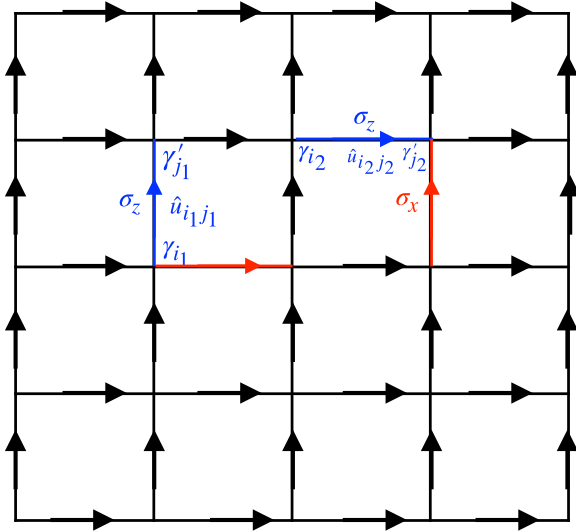


FIG. 10. The fermionization of the model in Eq. (B1). The links that Pauli matrices  $Z_i, X_{i+\delta}$  act upon are colored in blue and red, respectively. There are two Majorana degrees of freedom,  $\gamma_{v_i}, \gamma'_{v_i}$ , on each lattice site  $v_i$  in the fermionized Hilbert space, corresponding to the  $f$  anyon in the toric code model and we implicitly assume that the location of the  $f$  anyon is the same as the comprising  $e$  anyon. The term  $Z_i X_{i+\delta}$  is fermionized as  $i u_i \gamma_{v_i} \gamma'_{v'_i}$ , where  $v_i, v'_i$  are the starting point and the end point of the link  $i$ , with the direction defined by the arrows, and  $u_i$  is a static  $Z_2$  gauge field on link  $i$ , which accounts for the mutual semion statistics between  $f$  anyons (fermions) and  $m$  anyons ( $Z_2$  flux).

Besides,  $Z_i X_{i+\delta}$  and  $A_v, B_p$  satisfy an additional relation:

$$\prod_{i \in \partial p} Z_i X_{i+\delta} = B_p A_{v=p+\delta}. \quad (\text{B6})$$

Under the mapping in Eq. (B3), the left-hand side of Eq. (B6) is mapped to  $\prod_{i \in \partial p} T_{v_i v'_i} = (1 - 2n_{p-\delta}^f)(1 - 2n_{p+\delta}^f) \prod_{i \in \partial p} \hat{u}_i$ . The right-hand side of Eq. (B6) can be rewritten as  $W_p A_{p-\delta} B_{p+\delta}$ . Then, Eq. (B6) together with the Eq. (B2) determine the  $Z_2$  flux configuration in the fermion model,

$$\prod_{i \in \partial p} \hat{u}_i \longleftrightarrow A_{p-\delta} B_p = W_p, \quad (\text{B7})$$

as expected. Equations (B2), (B3), and (B7) form the complete the dictionary of the fermionization procedure on an infinite lattice or a topologically trivial lattice. However, on the fermionic side, under periodic boundary conditions,

i.e., on a torus, there are additional  $Z_2$  fluxes threading the two noncontractible cycles  $\gamma_x, \gamma_y$  along the  $x$  and  $y$  direction:  $\hat{w}_{x,y} = \prod_{i \in \gamma_{x,y}} \hat{u}_i$ . We need to figure out what is the counterpart of  $\hat{w}_{x,y}$  on the toric code side. This can be done by again using the mapping in Eq. (B3), which leads to

$$-\left( \prod_{i \in \gamma_{x,y}} \hat{u}_i \right) \prod_{i \in \gamma_{x,y}} (1 - 2n_{v_i}^f) \longleftrightarrow \prod_{i \in \gamma_{x,y}} Z_i X_{i+\delta}. \quad (\text{B8})$$

By using Eq. (B2), we obtain

$$-\hat{w}_{x(y)} \longleftrightarrow \prod_{i \in \gamma_{x(y)}} A_{v_i} Z_i X_{i+\delta} = \prod_{i \in \gamma_{x(y)}} Z_i X_{i-\delta} \equiv \hat{W}_{\gamma_{x(y)}}^{f'}. \quad (\text{B9})$$

Indeed,  $\hat{W}_{\gamma_x}^{f'}$  and  $\hat{W}_{\gamma_y}^{f'}$  are also conserved quantities in the original model,  $[\hat{W}_{\gamma_{x(y)}}^{f'}, H] = 0$ .

In the end, we map the model in Eq. (B1) to a quadratic fermion model with static  $Z_2$  gauge field,

$$H \leftrightarrow \tilde{H} = \sum_v (2n_v^f - 1)(1 + \hat{w}_p) - h_{xz} \sum_{(vv')} i \hat{u}_{vv'} \gamma_v \gamma'_{v'}, \quad (\text{B10})$$

where  $\hat{w}_p = \prod_{(vv') \in \partial p} \hat{u}_{vv'}$ .

Due to the extensive number of conserved quantities,  $[\hat{u}_{vv'}, \tilde{H}] = [\hat{w}_{p/x/y}, \tilde{H}] = 0$ ,  $\tilde{H}$  can be reduced to a free fermion model in each  $Z_2$  flux sector,  $\{\hat{w}_p = w_p, \hat{w}_x = w_x, \hat{w}_y = w_y\}$ , and thus can be easily solved. In the case  $h_{xz} = 0$ , it is obvious that the ground state (the vacuum of  $f$ ) lies in the zero-flux sector  $w_p = 1$  and the lowest energy state in the four sectors with distinct  $\{w_x = \pm 1, w_y = \pm 1\}$  has degenerate eigenenergy. This is just another perspective on the well-known topological degeneracy.

Via numerical investigations, we find that the ground state always stays in the sector with  $w_p = 1$ , irrespective of the value of  $h_{xz}$ , so we will mainly restrict our discussion to this case,

$$\tilde{H} = 4 \sum_v n_v^f - h_{xz} \sum_{(vv')} f_v^\dagger f_{v'} + f_v f_{v'} + \text{h.c.}, \quad (\text{B11})$$

and  $w_a = 1, -1$  ( $a = x, y$ ) corresponds to PBC and APBC, respectively, along direction  $a$ . Then,  $\tilde{H}$  can be solved via Fourier transformation,  $f_v = (1/\sqrt{L_x L_y}) \sum_{k_a = (2n_a \pi / L_a)} f_k e^{i k_x v_x + i k_y v_y}$ , where  $n \in \mathbb{Z}$  for PBC and  $n \in \mathbb{Z} + \frac{1}{2}$  for APBC:

$$\tilde{H} = \sum_k (f_k^\dagger, f_{-k}) \begin{pmatrix} 2 - h_{xz}(\cos k_x + \cos k_y) & -i h_{xz}(\sin k_x + \sin k_y) \\ i h_{xz}(\sin k_x + \sin k_y) & -2 + h_{xz}(\cos k_x + \cos k_y) \end{pmatrix} \begin{pmatrix} f_k \\ f_{-k}^\dagger \end{pmatrix}. \quad (\text{B12})$$

The dispersion of Bogoliubov quasiparticle excitation can easily be obtained,

$$\xi_k = 2\sqrt{[2 - h_{xz}(\cos k_x + \cos k_y)]^2 + [h_{xz}(\sin k_x + \sin k_y)]^2}, \quad (\text{B13})$$

and the ground-state energy is  $E_g = -\sum_k \xi_k/2$ . For  $h_{xz} < 1$ , the spectrum is gapped and the ground energy is nearly degenerate (with an exponentially small splitting) for the four types of boundary conditions. This corresponds to the gapped topologically ordered phase of  $H$ . For  $h_{xz} = 1$ , the gap closes at  $k_x = k_y = 0$  and remains closed for  $h_{xz} > 1$ , with linear dispersion at two Dirac points,  $k_x = -k_y = \pm \arccos(1/h_{xz})$ . So for  $h_{xz} > 1$ , the original model lies in a gapless spin liquid phase, reminiscent of the gapless phase of the Kitaev honeycomb model. In this phase, the topological degeneracy is lifted by an algebraically small gap but the ground state remains long-range entangled.

### APPENDIX C: DETAILS OF THE DECOHERED KITAEV HONEYCOMB MODEL

#### 1. The model

In this appendix, we provide a detailed analysis of the effect of proliferation of the  $f$  anyons in the Kitaev honeycomb model at zero magnetic field:

$$H = -J_x \sum_{x \text{ bonds}} \sigma_j^x \sigma_k^x - J_y \sum_{y \text{ bonds}} \sigma_j^y \sigma_k^y - J_z \sum_{z \text{ bonds}} \sigma_j^z \sigma_k^z. \quad (\text{C1})$$

This can be exactly solved by introducing the Majorana fermion operators:  $\sigma^\alpha = ib^\alpha b^0$ . After fixing the  $Z_2$  gauge fields as  $\hat{u}_{jk} = ib_j^\alpha b_k^\alpha = 1$  (which corresponds to the zero-gauge-flux sector in which the ground state lies), the Kitaev Hamiltonian given in Eq. (C1) becomes the following quadratic fermion model:

$$H_F = -J_x \sum_{x \text{ bonds}} b_j^x b_k^x - J_y \sum_{y \text{ bonds}} b_j^y b_k^y - J_z \sum_{z \text{ bonds}} b_j^z b_k^z, \quad (\text{C2})$$

the ground state  $|\psi_F\rangle$  of which can be easily solved. The physical ground state  $|\Psi\rangle$  can be obtained by projection to the gauge-invariant subspace using the projection operator  $\hat{P} = \Pi_i((1 + \hat{D}_i)/2)$ , i.e.,  $|\Psi\rangle = \Pi_i((1 + \hat{D}_i)/2)|\{u_{ij} = 1\}\rangle \otimes |\psi_F\rangle$ , where  $\hat{D}_i = b_i^x b_i^y b_i^z b_i^0$ . We will focus on the Abelian phase with  $|J_z| > |J_x| + |J_y|$ , where  $H_F$  is trivially gapped and  $|\Psi\rangle$  belongs to the  $Z_2$  TO.

The effect of the noisy channel in Eq. (26) is to change the fermion part of the density matrix but leave the gauge-field configuration invariant. This can be shown by writing the Kraus operators in terms of Majorana-fermion operators:  $\sigma_i^\alpha \sigma_j^\alpha = -i\hat{u}_{ij} b_i^0 b_j^0$ . Thus the density matrix  $\rho_f$  can

be written as

$$\rho_f = \hat{P}|\{u_{ij} = 1\}\rangle\langle\{u_{ij} = 1\}| \otimes \rho_F \hat{P}, \quad (\text{C3})$$

where  $\rho_F$  is the Majorana-fermion density matrix, which is  $\rho_F = \mathcal{N}^{X,F} \circ \mathcal{N}^{Y,F} \circ \mathcal{N}^{Z,F} [\rho_{F,0}]$ , where  $\rho_{F,0} = |\psi_F\rangle\langle\psi_F|$  is the ground state of  $H_F$ .  $\mathcal{N}^{\alpha,F} = \prod_{\langle ij \rangle} \mathcal{N}_{\langle ij \rangle}^{\alpha,F}$ , with

$$\mathcal{N}_{\langle ij \rangle \in \alpha \text{ bonds}}^{\alpha,F} [\cdot] \equiv (1-p) \cdot + p b_i^0 b_j^0 \cdot b_j^0 b_i^0. \quad (\text{C4})$$

Similar to the case of the toric code model, we expect that the error-corrupted state  $\rho_f$  undergoes a phase transition in the mixed-state topological order at some critical error rate  $p_c$ . In the limit  $|J_z| \gg |J_x|, |J_y|$ ,  $p_c$  can be determined by mapping to the RBIM, analogous to the case of the toric code, which gives  $p_c \approx 0.109$ . The topological quantum memory also breaks down to classical topological memory after the transition, with two remaining commuting logical operators:

$$W_{\gamma_x} = \prod_{\langle ij \rangle \in \gamma_x} \sigma_i^{\alpha_{\langle ij \rangle}} \sigma_j^{\alpha_{\langle ij \rangle}}, \quad W_{\gamma_y} = \prod_{\langle ij \rangle \in \gamma_y} \sigma_i^{\alpha_{\langle ij \rangle}} \sigma_j^{\alpha_{\langle ij \rangle}}, \quad (\text{C5})$$

where  $\alpha_{\langle ij \rangle} = x, y, z$  for  $\langle ij \rangle \in x$  bonds,  $y$  bonds, and  $z$  bonds. The two logical operators are depicted in Fig. 5. The residual classical memory is due to the fact that  $[W_{\gamma_x}, \sigma_i^{\alpha_{\langle ij \rangle}} \sigma_j^{\alpha_{\langle ij \rangle}}] = [W_{\gamma_y}, \sigma_i^{\alpha_{\langle ij \rangle}} \sigma_j^{\alpha_{\langle ij \rangle}}] = 0$ ,  $\forall \langle ij \rangle$ .

#### 2. Entanglement negativity

In this section, we compute the entanglement negativity of the  $\rho_f$  in the decohered Kitaev honeycomb model, starting from the Abelian phase. We will demonstrate the existence of a nonzero TEN for any error rate  $p$ .

Again, we use the replica trick to compute the entanglement negativity:

$$\mathcal{E}_A(\rho_f) := \log \left\| \rho_f^{T_A} \right\|_1 = \lim_{2n \rightarrow 1} \frac{1}{2-2n} \log \frac{\text{Tr} \left( \rho_f^{T_A} \right)^{2n}}{\text{Tr} \rho_f^{2n}}. \quad (\text{C6})$$

First, it is easy to show that  $\lim_{2n \rightarrow 1} \text{Tr} \rho_f^{2n} = \text{Tr} \rho_f = 1$ , due to the trace-preserving property of quantum channels.

So we only need to deal with the numerator:  $\text{Tr} \left( \rho_f^{T_A} \right)^{2n}$ .

A general curve  $\gamma$ , which bipartites the honeycomb lattice into subregions  $A$  and  $B = \bar{A}$ , intersects the bonds of the honeycomb lattice. In order to partially transpose the degrees of freedom in subregion  $A$ , we should define new  $Z_2$  gauge fields to replace the gauge fields on the intersected bonds. Following the notation in Ref. [115], we assume that  $\gamma$  intersects  $2L$  bonds and we denote the bonds intersected by the curve  $\gamma$  as  $\langle a_n b_n \rangle, n = 1, 2, \dots, 2L$ . If the  $Z_2$  gauge field on the bonds  $\langle a_{2n-1} b_{2n-1} \rangle$  and

$\langle a_{2n}b_{2n} \rangle$  are  $\hat{u}_{a_{2n-1}b_{2n-1}} = ib_{a_{2n-1}}^\alpha b_{b_{2n-1}}^\alpha$ ,  $\hat{u}_{a_{2n}b_{2n}} = ib_{a_{2n}}^\beta b_{b_{2n}}^\beta$ , then we introduce two  $Z_2$  gauge fields in subregions  $A$  and  $B$ , respectively:  $w_{A,n} = ib_{a_{2n-1}}^\alpha b_{a_{2n}}^\beta$ ,  $w_{B,n} = ib_{b_{2n-1}}^\beta b_{b_{2n}}^\alpha$ . Then the ground-state configuration of the gauge fields on the intersected links can be written as:

$$|\{u_p\}\rangle = \frac{1}{\sqrt{2^L}} \sum_{w_A=w_B=\{\pm 1\}} |w_A, w_B\rangle, \quad (C7)$$

where  $|\{u_p\}\rangle$  is the direct product of  $|u_{a_n b_n} = 1\rangle$ . As a result, the ground-state density matrix can be written as

$$\rho_0 = \frac{1}{2^{N+L+1}} \sum_{g,g',w,w'} D_g |u_A, w\rangle |u_B, w\rangle \langle u_A, w'| \langle u_B, w'| \otimes \rho_{F,0} D_{g'}, \quad (C8)$$

where the summation over  $g$  and  $g'$  is over all the possible sets of the lattice sites and  $D_g = \prod_{i \in g} D_i$ . What is more, we can simply replace the  $\rho_{F,0}$  with  $\rho_F$  to obtain the decohered density matrix  $\rho_f$ . The partial trace of the density matrix is

$$\rho_f^{TA} = \frac{1}{2^{N+L+1}} \sum_{g,g',w,w'} D_{g'} D_{g_B} |u_A, w'\rangle |u_B, w\rangle \langle u_A, w| \langle u_B, w'| \otimes \rho_F^{TA} D_{g_A} D_{g_A}. \quad (C9)$$

Thus,

$$\begin{aligned} (\rho_f^{TA})^2 &= \left( \frac{1}{2^{N+L+1}} \right)^2 \sum_{g,g',w,w'} \sum_{g_2, g_2', w_2, w_2'} \\ & D_{g_A'} D_{g_B} \left( |u_A, w'\rangle |u_B, w\rangle \otimes \rho_F^{TA} \right) \langle u_A, w| \langle u_B, w'| D_{g_B'} D_{g_A} D_{g_{2,B}} D_{g_{2,A}'} |u_A, w_2'\rangle |u_B, w_2\rangle \\ & \langle u_A, w_2| \langle u_B, w_2'| \otimes \left( \rho_F^{TA} \right) D_{g_{2,B}} D_{g_{2,A}} \end{aligned} \quad (C10)$$

where  $g_A$  and  $g_B$ , are the sets of lattice sites  $g \cap A$  and  $g \cap B$ , respectively. Now, we split  $D_g$  into the gauge-field part and the fermion part:  $D_g = X_g Y_g$ , where  $X_g = i^{|\mathcal{g}|(|\mathcal{g}|-1)/2} \prod_{j \in \mathcal{g}} b_j^\dagger b_j^\dagger b_j^\dagger$  and  $Y_g = i^{|\mathcal{g}|(|\mathcal{g}|-1)/2} \prod_{j \in \mathcal{g}} b_j^0$ , where  $|\mathcal{g}|$  is the number of lattice sites in region  $g$ . The inner product can be simplified as

$$\begin{aligned} & \langle u_A, w| \langle u_B, w'| D_{g_B'} D_{g_A} D_{g_{2,B}} D_{g_{2,A}'} |u_A, w_2'\rangle |u_B, w_2\rangle \\ &= \delta_{w,w_2'} \left( \delta_{g_A, g_{2,A}'} + x_A(w) \delta_{g_A, A-g_{2,A}'} Y_A \right) \delta_{w', w_2} \left( \delta_{g_B, g_{2,B}} + x_A(w) \delta_{g_B, B-g_{2,B}} Y_B \right) \\ &= \left( 2\delta_{w,w_2'} P_{F,A}^{x_A(w)} \right) \left( 2\delta_{w', w_2} P_{F,B}^{x_B(w')} \right), \end{aligned} \quad (C11)$$

where  $P_{F,A(B)}^x = ((1 + xY_{A(B)})/2)$  is the projection to the subspace with fixed Fermi parity  $x$  in subregion  $A$  ( $B$ ), and  $x_{A(B)}(w) = \langle u_{A(B)}, w | X_{A(B)} | u_{A(B)}, w \rangle = p_{A(B)} \prod_{n=1}^L w_n$ , where we define  $p_{A(B)} \equiv \prod_{i,j \in A(B)} u_{ij}$ . Putting this inner product back into  $(\rho_f^{TA})^2$ , we obtain

$$\begin{aligned} (\rho_f^{TA})^2 &= \left( \frac{1}{2^{N+L+1}} \right)^2 \sum_{g,g',w,w'} D_g |u_A, w'\rangle |u_B, w\rangle \langle u_A, w'| \langle u_B, w| \otimes \rho_F^{TA} 2^N \left( 2P_{F,A}^{x_A(w)} \right) \left( 2P_{F,B}^{x_B(w')} \right) \rho_F^{TA} D_{g'} \\ &= \frac{1}{2^{N+2L}} \sum_{g,g',w,w'} D_g |u_A, w'\rangle |u_B, w\rangle \langle u_A, w'| \langle u_B, w| \otimes \rho_F^{TA} P_{F,A}^{x_A(w)} P_{F,B}^{x_B(w')} \rho_F^{TA} D_{g'}. \end{aligned} \quad (C12)$$

We now move one step further to calculate  $(\rho_f^{TA})^4$ :



$$\begin{aligned}
(\rho_f^{T_A})^4 &= ((\rho^{T_A})^2)^2 = \left(\frac{1}{2^{N+2L}}\right)^2 \sum_{g,g',w,w'} D_g |u_A, w'\rangle |u_B, w\rangle \langle u_A, w'| \langle u_B, w| \otimes \rho_F^{T_A} P_{F,A}^{x_A(w)} P_{F,B}^{x_B(w')} \rho_F^{T_A} D_{g'} \\
&\quad \sum_{g_2, g'_2, w_2, w'_2} D_{g_2} |u_A, w'_2\rangle |u_B, w_2\rangle \langle u_A, w'_2| \langle u_B, w_2| \otimes \rho_F^{T_A} P_{F,A}^{x_A(w_2)} P_{F,B}^{x_B(w'_2)} \rho_F^{T_A} D_{g'_2} \\
&= \left(\frac{1}{2^{N+2L}}\right)^2 \sum_{g,g',w,w'} D_g |u_A, w'\rangle |u_B, w\rangle \langle u_A, w'| \langle u_B, w| \otimes \rho_F^{T_A} P_{F,A}^{x_A(w)} P_{F,B}^{x_B(w')} \rho_F^{T_A} \\
&\quad 2^N \left(2P_{F,A}^{x_A(w')}\right) \left(2P_{F,B}^{x_B(w)}\right) \rho_F^{T_A} P_{F,A}^{x_A(w)} P_{F,B}^{x_B(w')} \rho_F^{T_A} D_{g'} \\
&= \frac{1}{2^{N+4L-2}} \sum_{g,g',w,w'} D_g |u_A, w'\rangle |u_B, w\rangle \langle u_A, w'| \langle u_B, w| \\
&\quad \otimes \left(\rho_F^{T_A} P_{F,A}^{x_A(w)} P_{F,B}^{x_B(w')}\right) \left(\rho_F^{T_A} P_{F,A}^{x_A(w')} P_{F,B}^{x_B(w)}\right) \left(\rho_F^{T_A} P_{F,A}^{x_A(w)} P_{F,B}^{x_B(w')}\right) \rho_F^{T_A} D_{g'}. \tag{C13}
\end{aligned}$$

With these results, we can now arrive at  $(\rho^{T_A})^{2n}$  by iteration and induction:

$$\begin{aligned}
(\rho_f^{T_A})^{2n} &= \frac{1}{2^{N+2nL-2(n-1)}} \sum_{g,g',w,w'} D_g |u_A, w'\rangle |u_B, w\rangle \langle u_A, w'| \langle u_B, w| \\
&\quad \left[ \left(\rho_F^{T_A} P_{F,A}^{x_A(w)} P_{F,B}^{x_B(w')}\right) \left(\rho_F^{T_A} P_{F,A}^{x_A(w')} P_{F,B}^{x_B(w)}\right) \right]^{n-1} \left(\rho_F^{T_A} P_{F,A}^{x_A(w)} P_{F,B}^{x_B(w')}\right) D_{g'}. \tag{C14}
\end{aligned}$$

Using Eq. (C11) again, we can obtain the trace:

$$\begin{aligned}
\text{Tr}(\rho_f^{T_A})^{2n} &= \frac{1}{2^{2nL-2n}} \sum_{w,w'} \text{Tr}_F \left( \rho_F^{T_A} P_{F,A}^{x_A(w')} P_{F,B}^{x_B(w)} \rho_F^{T_A} P_{F,A}^{x_A(w)} P_{F,B}^{x_B(w')} \right)^n \\
&= \frac{2^{L-1} \times 2^{L-1}}{2^{2n(L-1)}} \text{Tr}_F \left( \rho_F^{T_A} P_{F,A}^{p_A} P_{F,B}^{p_B} \rho_F^{T_A} P_{F,A}^{p_A} P_{F,B}^{p_B} + \rho_F^{T_A} P_{F,A}^{p_A} P_{F,B}^{-p_B} \rho_F^{T_A} P_{F,A}^{-p_A} P_{F,B}^{p_B} \right. \\
&\quad \left. + \rho_F^{T_A} P_{F,A}^{-p_A} P_{F,B}^{p_B} \rho_F^{T_A} P_{F,A}^{p_A} P_{F,B}^{-p_B} + \rho_F^{T_A} P_{F,A}^{-p_A} P_{F,B}^{-p_B} \rho_F^{T_A} P_{F,A}^{p_A} P_{F,B}^{p_B} \right)^n. \tag{C15}
\end{aligned}$$

Since the projector  $D_{\text{tot}} = \prod_i D_i = X_{\text{tot}} Y_{\text{tot}} = 1$ , the total fermion parity of the whole system is fixed by  $Y_{\text{tot}} = X_{\text{tot}} = p_A p_B$ .

Therefore, the terms in the bracket can be simplified as

$$\begin{aligned}
&\rho_F^{T_A} P_{F,A}^{p_A} P_{F,B}^{p_B} \rho_F^{T_A} P_{F,A}^{p_A} P_{F,B}^{p_B} + \rho_F^{T_A} P_{F,A}^{p_A} P_{F,B}^{-p_B} \rho_F^{T_A} P_{F,A}^{-p_A} P_{F,B}^{p_B} + \rho_F^{T_A} P_{F,A}^{-p_A} P_{F,B}^{p_B} \rho_F^{T_A} P_{F,A}^{p_A} P_{F,B}^{-p_B} + \rho_F^{T_A} P_{F,A}^{-p_A} P_{F,B}^{-p_B} \rho_F^{T_A} P_{F,A}^{p_A} P_{F,B}^{p_B} \\
&= \rho_F^{T_A} (P_{F,A}^+ + P_{F,A}^-) (P_{F,B}^+ + P_{F,B}^-) \rho_F^{T_A} (P_{F,A}^+ + P_{F,A}^-) (P_{F,B}^+ + P_{F,B}^-) \\
&= (\rho_F^{T_A})^2. \tag{C16}
\end{aligned}$$

Then, we can finally obtain the entanglement negativity:

$$\begin{aligned}
\mathcal{E}_A(\rho_f) &= \log(\text{tr}(\rho_f^{T_A})) \\
&= \lim_{2n \rightarrow 1} \frac{1}{2 - 2n} \log \text{tr} (\rho^{T_A})^{2n} \\
&= L \log 2 - \log 2 + \log \|\rho_F^{T_A}\|_1, \tag{C17}
\end{aligned}$$

where the last term is the entanglement negativity  $\varepsilon_A(\rho_F)$  of the density matrix of fermions. We note that the above result holds for any parameters  $J_x, J_y$ , and  $J_z$ , and also for general bipartitions as long as the length of the boundary is even ( $N_l = 2L$ ) and  $A$  and  $B$  are connected. To analyze the scaling behavior of  $\varepsilon_A$ , we again consider bipartition of a cylinder with a translation-invariant entanglement cut. In the gapped phase,  $\rho_{F,0}$  is a Gaussian state with finite correlation length, so  $\varepsilon_A(\rho_{F,0}) = \alpha L + \dots$  satisfies an area law, with a vanishing subleading term for  $L \rightarrow \infty$ . We expect  $\varepsilon_A(\rho_F)$  also to have the same property after applying local channels on  $\rho_F$ , since local quantum channels cannot generate long-range entanglement. Thus we obtain  $\text{TEN} = \log 2$ , consistent with our expectation for even boundary sizes, which shows that this result holds for mixed-state topological order beyond stabilizer codes. For the decohered Kitaev honeycomb model, we still anticipate the TEN to depend on the parity of  $N_l$ , as in the toric code model. Indeed, in the case  $p = \frac{1}{2}$ ,  $\rho_f$  is equivalent to  $\rho_f$  up to an on-site unitary transformation. However, for general  $p$ , the calculation of negativity for odd  $N_l$  is more complicated and thus is not shown here.

#### APPENDIX D: A PROOF THAT $e^2m^2$ IS A DECONFINED ANYON

In this appendix, we prove that  $e^2m^2$  indeed becomes a deconfined anyon in the decohered double-semion model, according to Definition 1. To start with, we write down the explicit form of the decohered state  $\rho = \mathcal{N}^{[em]}[\rho_0]$ , with maximal decoherence  $p_0 = p_1 = p_2 = p_3 = \frac{1}{4}$ . As discussed below Eq. (32),  $\rho$  is determined by the stabilizer group  $G = \{\{W_p^{e^3m}\}, \text{nonlocal stabilizers}\}$ :

$$\rho = \frac{1}{4^N} \sum_{g \in G} g. \quad (\text{D1})$$

We define the open  $e^2m^2$  string  $W_{\tilde{C}}^{e^2m^2} = \prod_{i \in \tilde{C}} X_i^2 Z_{i+\delta}^2$  on the dual lattice and  $U_{\tilde{C}} = (I + iW_{\tilde{C}}^{e^2m^2})/\sqrt{2}$ . Then,  $e^2m^2$  anyons can be created at  $\partial\tilde{C}$  by  $\rho \rightarrow U_{\tilde{C}}\rho U_{\tilde{C}}^\dagger$ . We prove below that both criteria in the definition of deconfined excitations are satisfied. The second criterion directly follows from the fact that  $e^2m^2$  anyons generate a strong 1-form symmetry of  $\rho$ , similar to the proof of the deconfinement of  $f$  anyons in Sec. III. The first criterion can be proved by contradiction. We assume that  $e^2m^2$  anyons can be locally created, i.e.,  $\exists V_{\partial\tilde{C}}$  supported near  $\partial\tilde{C}$ , such that  $U_{\tilde{C}}\rho U_{\tilde{C}}^\dagger = V_{\partial\tilde{C}}\rho V_{\partial\tilde{C}}^\dagger$ . Then, we define two noncontractible Wilson loops  $W_{\gamma_1}^e = \prod_{i \in \gamma_1} Z_i$  and  $W_{\gamma_2}^e = \prod_{i \in \gamma_2} Z_i^\dagger$ , as depicted in Fig. 11. Because the  $W_{\gamma_1}^e W_{\gamma_2}^e$  commute with  $V_{\partial\tilde{C}}$  as well as all the stabilizers, we have

$$W_{\gamma_1}^e W_{\gamma_2}^e V_{\partial\tilde{C}} \rho V_{\partial\tilde{C}}^\dagger W_{\gamma_1}^{e\dagger} W_{\gamma_2}^{e\dagger} = V_{\partial\tilde{C}} \rho V_{\partial\tilde{C}}^\dagger. \quad (\text{D2})$$

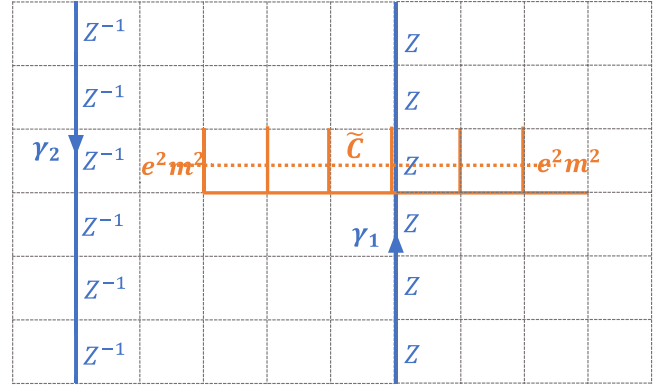


FIG. 11. Detecting  $e^2m^2$  anyons using Wilson loops.

On the other hand,  $W_{\gamma_1}^e W_{\gamma_2}^e$  anticommutes with  $W_{\tilde{C}}^{e^2m^2}$ , so

$$W_{\gamma_1}^e W_{\gamma_2}^e U_{\tilde{C}} \rho U_{\tilde{C}}^\dagger W_{\gamma_1}^{e\dagger} W_{\gamma_2}^{e\dagger} = U_{\tilde{C}}^\dagger \rho U_{\tilde{C}} \neq U_{\tilde{C}} \rho U_{\tilde{C}}^\dagger, \quad (\text{D3})$$

which leads to a contradiction with Eq. (D2). Therefore, the  $e^2m^2$  anyons cannot be locally created, so they are deconfined excitations in the decohered double-semion model.

- 
- [1] X. G. WEN, Topological orders in rigid states, *Int. J. Mod. Phys. B* **04**, 239 (1990).
  - [2] X. Chen, Z.-C. Gu, and X.-G. Wen, Local unitary transformation, long-range quantum entanglement, wave function renormalization, and topological order, *Phys. Rev. B* **82**, 155138 (2010).
  - [3] X.-G. Wen, Colloquium: Zoo of quantum-topological phases of matter, *Rev. Mod. Phys.* **89**, 041004 (2017).
  - [4] L. Savary and L. Balents, Quantum spin liquids: A review, *Rep. Prog. Phys.* **80**, 016502 (2016).
  - [5] Y. Zhou, K. Kanoda, and T.-K. Ng, Quantum spin liquid states, *Rev. Mod. Phys.* **89**, 025003 (2017).
  - [6] S. Sachdev, Topological order, emergent gauge fields, and Fermi surface reconstruction, *Rep. Prog. Phys.* **82**, 014001 (2018).
  - [7] M. Aguado, G. K. Brennen, F. Verstraete, and J. I. Cirac, Creation, manipulation, and detection of abelian and non-Abelian anyons in optical lattices, *Phys. Rev. Lett.* **101**, 260501 (2008).
  - [8] R. Verresen, M. D. Lukin, and A. Vishwanath, Prediction of toric code topological order from Rydberg blockade, *Phys. Rev. X* **11**, 031005 (2021).
  - [9] L. Piroli, G. Styliaris, and J. Ignacio Cirac, Quantum circuits assisted by local operations and classical communication: Transformations and phases of matter, *Phys. Rev. Lett.* **127**, 220503 (2021).
  - [10] N. Tantivasadakarn, R. Thorngren, A. Vishwanath, and R. Verresen, Long-range entanglement from measuring symmetry-protected topological phases, *Phys. Rev. X* **14**, 021040 (2024).

- [11] N. Tantivasadakarn, R. Verresen, and A. Vishwanath, Shortest route to non-abelian topological order on a quantum processor, *Phys. Rev. Lett.* **131**, 060405 (2023).
- [12] N. Tantivasadakarn, A. Vishwanath, and R. Verresen, Hierarchy of topological order from finite-depth unitaries, measurement, and feedforward, *PRX Quantum* **4**, 020339 (2023).
- [13] J. Yeon Lee, W. Ji, Z. Bi, and M. Fisher, Decoding measurement-prepared quantum phases and transitions: From ising model to gauge theory, and beyond, arXiv preprint [arXiv:2208.11699](https://arxiv.org/abs/2208.11699).
- [14] S. Bravyi, I. Kim, A. Kliesch, and R. Koenig, Adaptive constant-depth circuits for manipulating non-Abelian anyons, arXiv preprint [arXiv:2205.01933](https://arxiv.org/abs/2205.01933).
- [15] T.-C. Lu, Z. Zhang, S. Vijay, and T. H. Hsieh, Mixed-state long-range order and criticality from measurement and feedback, *PRX Quantum* **4**, 030318 (2023).
- [16] G. Semeghini, H. Levine, A. Keesling, S. Ebadi, T. Wang, D. Bluvstein, R. Verresen, H. Pichler, M. Kalinowski, R. Samajdar, A. Omran, S. Sachdev, A. Vishwanath, M. Greiner, V. Vuletic, and M. Lukin, Probing topological spin liquids on a programmable quantum simulator, *Science* **374**, 1242 (2021).
- [17] K. J. Satzinger *et al.*, Realizing topologically ordered states on a quantum processor, *Science* **374**, 1237 (2021).
- [18] T. I. Andersen *et al.*, Non-Abelian braiding of graph vertices in a superconducting processor, *Nature* **618**, 264 (2023).
- [19] S. Xu *et al.*, Digital simulation of projective non-Abelian anyons with 68 superconducting qubits, *Chin. Phys. Lett.* **40**, 060301 (2023).
- [20] M. Iqbal, N. Tantivasadakarn, T. M. Gatterman, J. A. Gerber, K. Gilmore, D. Gresh, A. Hankin, N. Hewitt, C. V. Horst, M. Matheny, T. Mengle, B. Neyenhuis, A. Vishwanath, M. Foss-Feig, R. Verresen, and H. Dreyer, Topological order from measurements and feed-forward on a trapped ion quantum computer, arXiv preprint [arXiv:2302.01917](https://arxiv.org/abs/2302.01917).
- [21] M. Iqbal, N. Tantivasadakarn, R. Verresen, S. L. Campbell, J. M. Dreiling, C. Figgatt, J. P. Gaebler, J. Johansen, M. Mills, S. A. Moses, J. M. Pino, A. Ransford, M. Rowe, P. Siegfried, R. P. Stutz, M. Foss-Feig, A. Vishwanath, and H. Dreyer, Creation of non-Abelian topological order and anyons on a trapped-ion processor, arXiv preprint [arXiv:2305.03766](https://arxiv.org/abs/2305.03766).
- [22] J. Preskill, Quantum computing in the NISQ era and beyond, *Quantum* **2**, 79 (2018).
- [23] E. Dennis, A. Kitaev, A. Landahl, and J. Preskill, Topological quantum memory, *J. Math. Phys.* **43**, 4452 (2002).
- [24] H. Bombin, R. S. Andrist, M. Ohzeki, H. G. Katzgraber, and M. A. Martin-Delgado, Strong resilience of topological codes to depolarization, *Phys. Rev. X* **2**, 021004 (2012).
- [25] M. McGinley and N. R. Cooper, Fragility of time-reversal symmetry protected topological phases, *Nat. Phys.* **16**, 1181 (2020).
- [26] T.-S. Deng, L. Pan, Y. Chen, and H. Zhai, Stability of time-reversal symmetry protected topological phases, *Phys. Rev. Lett.* **127**, 086801 (2021).
- [27] Z. Wang, Q. Li, W. Li, and Z. Cai, Symmetry-protected topological edge modes and emergent partial time-reversal symmetry breaking in open quantum many-body systems, *Phys. Rev. Lett.* **126**, 237201 (2021).
- [28] C. de Groot, A. Turzillo, and N. Schuch, Symmetry protected topological order in open quantum systems, *Quantum* **6**, 856 (2022).
- [29] J. Yeon Lee, Y.-Z. You, and C. Xu, Symmetry protected topological phases under decoherence, arXiv preprint [arXiv:2210.16323](https://arxiv.org/abs/2210.16323).
- [30] J.-H. Zhang, Y. Qi, and Z. Bi, Strange correlation function for average symmetry-protected topological phases, arXiv preprint [arXiv:2210.17485](https://arxiv.org/abs/2210.17485).
- [31] R. Fan, Y. Bao, E. Altman, and A. Vishwanath, Diagnostics of mixed-state topological order and breakdown of quantum memory, *PRX Quantum* **5**, 020343 (2024).
- [32] Y. Bao, R. Fan, A. Vishwanath, and E. Altman, Mixed-state topological order and the errorfield double formulation of decoherence-induced transitions, arXiv preprint [arXiv:2301.05687](https://arxiv.org/abs/2301.05687).
- [33] J. Yeon Lee, C.-M. Jian, and C. Xu, Quantum criticality under decoherence or weak measurement, *PRX Quantum* **4**, 030317 (2023).
- [34] R. Ma and C. Wang, Average symmetry-protected topological phases, *Phys. Rev. X* **13**, 031016 (2023).
- [35] R. Ma, J.-H. Zhang, Z. Bi, M. Cheng, and C. Wang, Topological phases with average symmetries: The decohered, the disordered, and the intrinsic, arXiv preprint [arXiv:2305.16399](https://arxiv.org/abs/2305.16399).
- [36] C.-E. Bardyn, L. Wawer, A. Altland, M. Fleischhauer, and S. Diehl, Probing the topology of density matrices, *Phys. Rev. X* **8**, 011035 (2018).
- [37] L. Mao, F. Yang, and H. Zhai, Dissipation dynamics driven transitions of the density matrix topology, arXiv preprint [arXiv:2301.04345](https://arxiv.org/abs/2301.04345).
- [38] K. Su, N. Myerson-Jain, C. Wang, C.-M. Jian, and C. Xu, Higher-form symmetries under weak measurement, arXiv preprint [arXiv:2304.14433](https://arxiv.org/abs/2304.14433).
- [39] Z. Wang, X.-D. Dai, H.-R. Wang, and Z. Wang, Topologically ordered steady states in open quantum systems, arXiv preprint [arXiv:2306.12482](https://arxiv.org/abs/2306.12482).
- [40] Y.-J. Liu and S. Lieu, Dissipative phase transitions and passive error correction, *Phys. Rev. A* **109**, 022422 (2024).
- [41] F. A. Bais and J. K. Slingerland, Condensate-induced transitions between topologically ordered phases, *Phys. Rev. B* **79**, 045316 (2009).
- [42] L. Kong, Anyon condensation and tensor categories, *Nucl. Phys. B* **886**, 436 (2014). [arXiv:1307.8244](https://arxiv.org/abs/1307.8244).
- [43] F. J. Burnell, Anyon condensation and its applications, *Ann. Rev. Condens. Matter Phys.* **9**, 307 (2018).
- [44] P. W. Anderson, Resonating valence bonds: A new kind of insulator? *Mater. Res. Bull.* **8**, 153 (1973).
- [45] N. Read and B. Chakraborty, Statistics of the excitations of the resonating-valence-bond state, *Phys. Rev. B* **40**, 7133 (1989).
- [46] N. Read and S. Sachdev, Large- $N$  expansion for frustrated quantum antiferromagnets, *Phys. Rev. Lett.* **66**, 1773 (1991).
- [47] X. G. Wen, Mean-field theory of spin-liquid states with finite energy gap and topological orders, *Phys. Rev. B* **44**, 2664 (1991).

- [48] P. W. Anderson, The resonating valence bond state in  $\text{La}_2\text{CuO}_4$  and superconductivity, *Science* **235**, 1196 (1987).
- [49] T. Senthil and M. P. A. Fisher,  $Z_2$  gauge theory of electron fractionalization in strongly correlated systems, *Phys. Rev. B* **62**, 7850 (2000).
- [50] R. Moessner and S. L. Sondhi, Resonating valence bond phase in the triangular lattice quantum dimer model, *Phys. Rev. Lett.* **86**, 1881 (2001).
- [51] A. Yu. Kitaev, Fault-tolerant quantum computation by anyons, *Ann. Phys. (NY)* **303**, 2 (2003).
- [52] E. Fradkin and S. H. Shenker, Phase diagrams of lattice gauge theories with Higgs fields, *Phys. Rev. D* **19**, 3682 (1979).
- [53] Y. A. Lee and G. Vidal, Entanglement negativity and topological order, *Phys. Rev. A* **88**, 042318 (2013).
- [54] C. Castelnovo, Negativity and topological order in the toric code, *Phys. Rev. A* **88**, 042319 (2013).
- [55] X. Wen, P.-Y. Chang, and S. Ryu, Topological entanglement negativity in Chern-Simons theories, *J. High Energy Phys.* **2016**, 12 (2016).
- [56] X. Wen, S. Matsuura, and S. Ryu, Edge theory approach to topological entanglement entropy, mutual information, and entanglement negativity in Chern-Simons theories, *Phys. Rev. B* **93**, 245140 (2016).
- [57] A. Kitaev and J. Preskill, Topological entanglement entropy, *Phys. Rev. Lett.* **96**, 110404 (2006).
- [58] M. Levin and X.-G. Wen, Detecting topological order in a ground state wave function, *Phys. Rev. Lett.* **96**, 110405 (2006).
- [59] O. Hart and C. Castelnovo, Entanglement negativity and sudden death in the toric code at finite temperature, *Phys. Rev. B* **97**, 144410 (2018).
- [60] T.-C. Lu, T. H. Hsieh, and T. Grover, Detecting topological order at finite temperature using entanglement negativity, *Phys. Rev. Lett.* **125**, 116801 (2020).
- [61] T.-C. Lu, E.-J. Kuo, and H.-H. Lin, Entanglement cost in topological stabilizer models at finite temperature, arXiv preprint [arXiv:2201.08382](https://arxiv.org/abs/2201.08382).
- [62] T.-C. Lu and S. Vijay, Characterizing long-range entanglement in a mixed state through an emergent order on the entangling surface, arXiv preprint [arXiv:2201.07792](https://arxiv.org/abs/2201.07792).
- [63] D. Gaiotto, A. Kapustin, N. Seiberg, and B. Willett, Generalized global symmetries, *J. High Energy Phys.* **2015**, 172 (2015).
- [64] X.-G. Wen, Emergent anomalous higher symmetries from topological order and from dynamical electromagnetic field in condensed matter systems, *Phys. Rev. B* **99**, 205139 (2019).
- [65] J. McGreevy, Generalized symmetries in condensed matter, *Ann. Rev. Condens. Matter Phys.* **14**, 57 (2023).
- [66] L. A. Lessa, M. Cheng, and C. Wang, Mixed-state quantum anomaly and multipartite entanglement, arXiv preprint [arXiv:2401.17357](https://arxiv.org/abs/2401.17357).
- [67] R. Sohal and A. Prem, Noisy approach to intrinsically mixed-state topological order, *PRX Quantum* **6**, 010313 (2025).
- [68] T. D. Ellison and M. Cheng, Toward a classification of mixed-state topological orders in two dimensions, *PRX Quantum* **6**, 010315 (2025).
- [69] B. Schumacher and M. A. Nielsen, Quantum data processing and error correction, *Phys. Rev. A* **54**, 2629 (1996).
- [70] B. Schumacher and M. D. Westmoreland, Approximate quantum error correction, [arXiv:quant-ph/0112106](https://arxiv.org/abs/quant-ph/0112106).
- [71] H. Nishimori, Internal energy, specific heat and correlation function of the bond-random Ising model, *Prog. Theor. Phys.* **66**, 1169 (1981).
- [72] A. Peres, Separability criterion for density matrices, *Phys. Rev. Lett.* **77**, 1413 (1996).
- [73] M. Horodecki, P. Horodecki, and R. Horodecki, Separability of mixed states: Necessary and sufficient conditions, *Phys. Lett. A* **223**, 1 (1996).
- [74] K. Życzkowski, P. Horodecki, A. Sanpera, and M. Lewenstein, Volume of the set of separable states, *Phys. Rev. A* **58**, 883 (1998).
- [75] G. Vidal and R. F. Werner, Computable measure of entanglement, *Phys. Rev. A* **65**, 032314 (2002).
- [76] X.-G. Wen, Quantum orders in an exact soluble model, *Phys. Rev. Lett.* **90**, 016803 (2003).
- [77] A. Kitaev, Anyons in an exactly solved model and beyond, *Ann. Phys. (NY)* **321**, 2 (2006). January Special Issue.
- [78] C. Castelnovo and C. Chamon, Topological order and topological entropy in classical systems, *Phys. Rev. B* **76**, 174416 (2007).
- [79] C. Castelnovo and C. Chamon, Entanglement and topological entropy of the toric code at finite temperature, *Phys. Rev. B* **76**, 184442 (2007).
- [80] C. Castelnovo and C. Chamon, Topological order in a three-dimensional toric code at finite temperature, *Phys. Rev. B* **78**, 155120 (2008).
- [81] S. Trebst, P. Werner, M. Troyer, K. Shtengel, and C. Nayak, Breakdown of a topological phase: Quantum phase transition in a loop gas model with tension, *Phys. Rev. Lett.* **98**, 070602 (2007).
- [82] I. S. Tupitsyn, A. Kitaev, N. V. Prokof'ev, and P. C. E. Stamp, Topological multicritical point in the phase diagram of the toric code model and three-dimensional lattice gauge Higgs model, *Phys. Rev. B* **82**, 085114 (2010).
- [83] S. Dusuel, M. Kamfor, R. Orús, K. P. Schmidt, and J. Vidal, Robustness of a perturbed topological phase, *Phys. Rev. Lett.* **106**, 107203 (2011).
- [84] A. M. Somoza, P. Serna, and A. Nahum, Self-dual criticality in three-dimensional  $\mathbb{Z}_2$  gauge theory with matter, *Phys. Rev. X* **11**, 041008 (2021).
- [85] Y.-A. Chen, A. Kapustin, and D. Radicevic, Exact bosonization in two spatial dimensions and a new class of lattice gauge theories, *Ann. Phys. (NY)* **393**, 234 (2018).
- [86] E. Fradkin and J. E. Moore, Entanglement entropy of 2D conformal quantum critical points: Hearing the shape of a quantum drum, *Phys. Rev. Lett.* **97**, 050404 (2006).
- [87] H. Casini, M. Huerta, and L. Leitao, Entanglement entropy for a Dirac fermion in three dimensions: Vertex contribution, *Nucl. Phys. B* **814**, 594 (2009).
- [88] P. Bueno, R. C. Myers, and W. Witczak-Krempa, Universality of corner entanglement in conformal field theories, *Phys. Rev. Lett.* **115**, 021602 (2015).
- [89] This equality always holds for contractible  $\tilde{\gamma}$ , while for noncontractible  $\tilde{\gamma}$  it only holds for a particular choice

- of the initial state  $\rho_0$ :  $W_{\tilde{\gamma}}\rho_0 = \rho_0$ . Fortunately, for the argument below, we only need to use this condition for contractible  $\tilde{\gamma}$ , so this subtlety can be safely ignored.
- [90] B. Buca and T. Prosen, A note on symmetry reductions of the Lindblad equation: Transport in constrained open spin chains, *New J. Phys.* **14**, 073007 (2012). [arXiv:1203.0943](#).
- [91] S. Lieu, R. Belyansky, J. T. Young, R. Lundgren, V. V. Albert, and A. V. Gorshkov, Symmetry breaking and error correction in open quantum systems, *Phys. Rev. Lett.* **125**, 240405 (2020).
- [92] M. Levin and X.-G. Wen, Fermions, strings, and gauge fields in lattice spin models, *Phys. Rev. B* **67**, 245316 (2003).
- [93] Z. Wang and L. Li, Anomaly in open quantum systems and its implications on mixed-state quantum phases, arXiv preprint [arXiv:2403.14533](#).
- [94] Nevertheless, one can alternatively use the ancilla to control the creation of two  $f$  anyons and extract the braiding statistics by moving  $e$  around  $f$ .
- [95] Z. Li and R. S. K. Mong, Replica topological order in quantum mixed states and quantum error correction, arXiv preprint [arXiv:2402.09516](#).
- [96] M. B. Hastings, Topological order at nonzero temperature, *Phys. Rev. Lett.* **107**, 210501 (2011).
- [97] S. Sang, Y. Zou, and T. H. Hsieh, Mixed-state quantum phases: Renormalization and quantum error correction, *Phys. Rev. X* **14**, 031044 (2024).
- [98] J. Watrous, *The Theory of Quantum Information* (Cambridge University Press, Cambridge, 2018).
- [99] M. Levin and Z.-C. Gu, Braiding statistics approach to symmetry-protected topological phases, *Phys. Rev. B* **86**, 115109 (2012).
- [100] M. Levin, Protected edge modes without symmetry, *Phys. Rev. X* **3**, 021009 (2013).
- [101] R. Liu, H. Tat Lam, H. Ma, and L. Zou, Symmetries and anomalies of Kitaev spin- $S$  models: Identifying symmetry-enforced exotic quantum matter, *SciPost Phys.* **16**, 100 (2024).
- [102] K. Hwang, Mixed-state quantum spin liquid in Kitaev Lindbladian: Dynamical anyon condensation, arXiv preprint [arXiv:2305.09197](#).
- [103] M. A. Levin and X.-G. Wen, String-net condensation: A physical mechanism for topological phases, *Phys. Rev. B* **71**, 045110 (2005).
- [104] T. D. Ellison, Y.-A. Chen, A. Dua, W. Shirley, N. Tantivasadakarn, and D. J. Williamson, Pauli stabilizer models of twisted quantum doubles, *PRX Quantum* **3**, 010353 (2022).
- [105] T. D. Ellison, Y.-A. Chen, A. Dua, W. Shirley, N. Tantivasadakarn, and D. J. Williamson, Pauli topological subsystem codes from Abelian anyon theories, *Quantum* **7**, 1137 (2023).
- [106] L. Kong and X.-G. Wen, Braided fusion categories, gravitational anomalies, and the mathematical framework for topological orders in any dimensions, arXiv preprint [arXiv:1405.5858](#).
- [107] R. Dijkgraaf and E. Witten, Topological gauge theories and group cohomology, *Commun. Math. Phys.* **129**, 393 (1990).
- [108] Y. Hu, Y. Wan, and Y.-S. Wu, Twisted quantum double model of topological phases in two dimensions, *Phys. Rev. B* **87**, 125114 (2013).
- [109] J. C. Magdalena de la Fuente, N. Tarantino, and J. Eisert, Non-Pauli topological stabilizer codes from twisted quantum doubles, *Quantum* **5**, 398 (2021).
- [110] H. Song, N. Tantivasadakarn, W. Shirley, and M. Hermele, Fracton self-statistics, *Phys. Rev. Lett.* **132**, 016604 (2024).
- [111] For convenience, we drop the subscript of  $p_f$  in Appendixes A 1–A 4.
- [112] K. Fredenhagen and M. Marcu, Charged states in  $Z_2$  gauge theories, *Commun. Math. Phys.* **92**, 81 (1983).
- [113] K. Gregor, D. A. Huse, R. Moessner, and S. L. Sondhi, Diagnosing deconfinement and topological order, *New J. Phys.* **13**, 025009 (2011).
- [114] P. Rao and I. Sodemann, Theory of weak symmetry breaking of translations in  $Z_2$  topologically ordered states and its relation to topological superconductivity from an exact lattice  $Z_2$  charge-flux attachment, *Phys. Rev. Res.* **3**, 023120 (2021).
- [115] H. Yao and X.-L. Qi, Entanglement entropy and entanglement spectrum of the Kitaev model, *Phys. Rev. Lett.* **105**, 080501 (2010).